SPRING 2023
electronics-cooling.com

electronics COOLING

FEATURED IN THIS EDITION

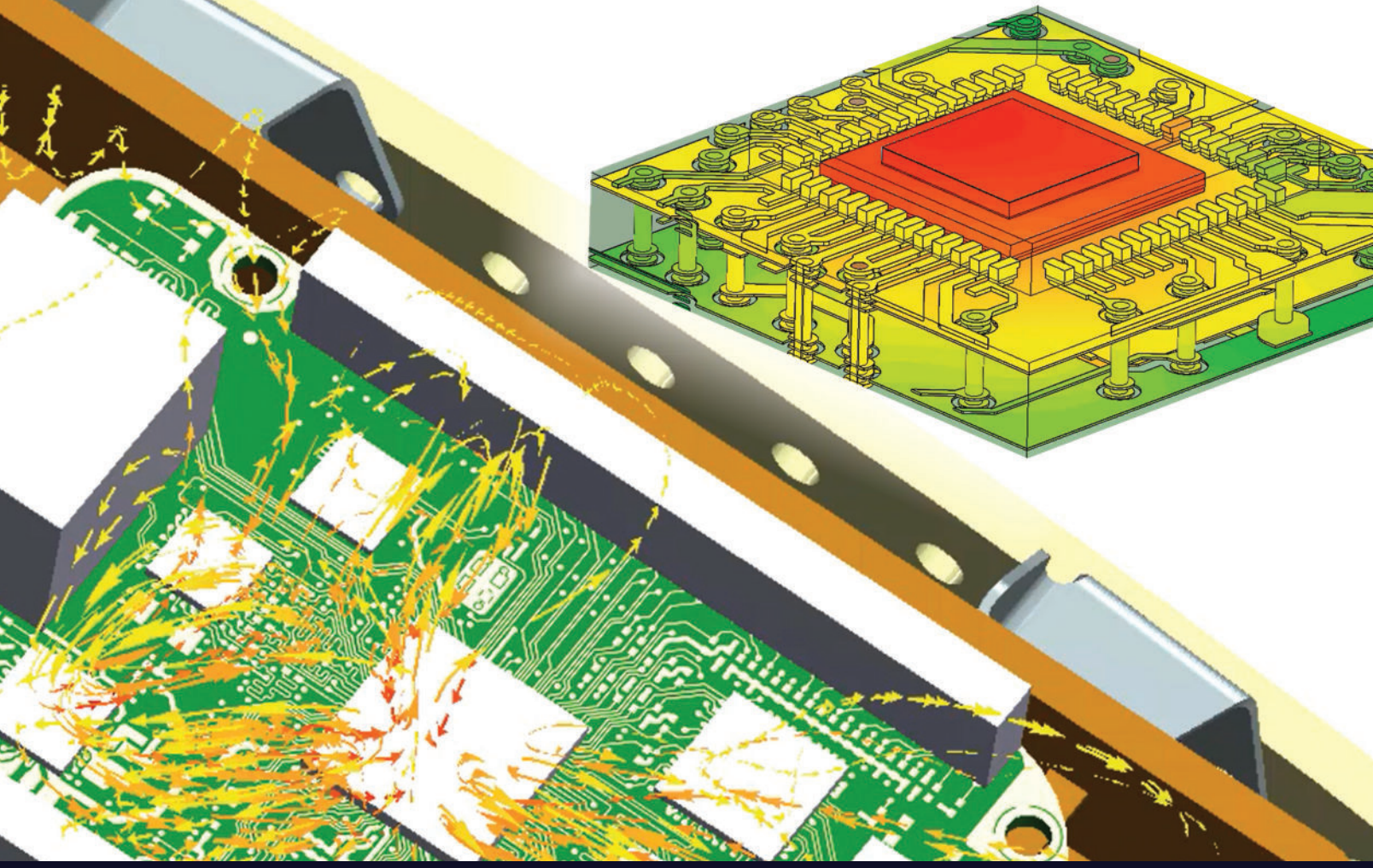

Accelerate thermal, thermo-mechanical and electro-thermal workflows

Leverage efficient CFD and FEA workflows for shorter, robust thermal and thermo-mechanical analysis. Underpin simulation accuracy with thermal measurement for characterization, calibration to reliability assessment. Incorporate EDA and MCAD data complexity efficiently into simulation. Enable PCB electro-thermal modeling using power integrity co-simulation. Realize the advantage of novel reduced order thermal model generation from full 3D analysis to improve accuracy in circuit or system modeling.

Simcenter provides simulation and test solutions to support you in developing a thermal digital twin. The portfolio includes a range of leading electronics cooling software , CAD-embedded CFD simulation options, and multi-physics analysis tools to support a wider range of user skill and experience demographic from analyst to designer. Learn how Siemens Digital Industries Software can help you achieve digital transformation goals.

www.siemens.com/simcenter

SIEMENS

CONTENTS

electronics COOLING
electronics-cooling.com

PUBLISHED BY
Lectrix
1000 Germantown Pike, F-2
Plymouth Meeting, PA 19462 USA
Phone: +1 484-688-0300; Fax:+1 484-688-0303
info@lectrixgroup.com
lectrixgroup.com

CHIEF EXECUTIVE OFFICER
Graham Kilshaw | graham@lectrixgroup.com

VP OF MARKETING
Geoffrey Forman | geoff@lectrixgroup.com

DIRECTOR OF MEDIA & EVENTS
Katherine Struve | katherine@lectrixgroup.com

DIRECTOR OF BUSINESS DEVELOPMENT
Ashlee Zapata-McCants | ashlee@lectrixgroup.com

CREATIVE DIRECTOR
Kate Teti | kate@lectrixgroup.com

DIRECTOR OF OPERATIONS
Stephanie Curry | stephanie@lectrixgroup.com

TRAFFIC COORDINATOR
Mackenzie Mann | mackenzie@lectrixgroup.com

CIRCULATION & ADMINISTRATION MANAGER
Eileen Ambler | eileen@lectrixgroup.com

►**SUBSCRIPTIONS ONLINE**
at electronics-cooling.com

For subscription changes email
info@electronics-cooling.com

FREE SUBSCRIPTIONS

Lectrix®, *Electronics Cooling®*—The **2023 Spring Edition** is distributed digitally at no charge to engineers and managers engaged in the application, selection, design, test, specification or procurement of electronic components, systems, materials, equipment, facilities or related fabrication services. Subscriptions are available through electronics-cooling.com.

LECTRIX®

EDITORIAL

Victor Chirac, PhD
Associate Technical Editor of *Electronics Cooling Magazine*
Co-founder and Managing Partner, Global Cooling Technology Group

Dear EC Readers,

Welcome to the Spring edition of our magazine. We are happy to share articles spanning double-sided cold plates, generative design and advanced 3D printing, guidelines for vapor chamber design, and applying advective thermal resistance to thermal resistance networks. The Statistics Corner describes a rank sum test for dealing with data that aren't necessarily from a normal distribution. We hope you'll enjoy these articles with your feedback being appreciated. I wish everyone a healthy and productive year!

This year, as we are moving to a full-digital edition of the ***Electronics Cooling Magazine*** with one issue per quarter, we plan to continue to keep you posted with the latest and greatest activities happening in our thermal community. Compared to last year, we see many changes following the Covid-19 pandemic, with very encouraging signs as the global industry rebounds and new technologies are being developed on multiple fronts, spanning from the semiconductor industry to medical/health care, consumer electronics, automotive and beyond.

Earlier this year I had the chance to "take the pulse" of the state of the technology world, by attending one of the most influential technology events: the Consumer Electronics Show, CES 2023 in Las Vegas, with over 118K attendants, over 3200 exhibitors, 930 speakers and 248 conference sessions. Aside from the main event, which hosted mid to large-sized global companies, the Eureka Park gathered over 1000 start-ups from around the world. Many innovative, groundbreaking technology solutions are coming from small to large companies that are solving critical problems for the humanity with thermal management being an important part of it. The major theme related to the role of technology is to make the world better, not only by addressing the needs for faster performance and reduced energy consumption, but also related to clean air, clean drinking water, improved and affordable healthcare, enhanced community engagement and communication.

It was interesting to see how the pandemic has accelerated the adoption of semiconductors, as chips become part of everyday life. High performance, adaptive and sustainable computing are critical for various walks of life and areas of society. The social revolution occurring these days shows that technology shapes us as much as we shape it, and the need for additional computational resources aligned with human intention and in the service of our communities is higher than ever.

As reported by many industrial outlets, Artificial Intelligence (AI) is one of the main defining trends in the technology world. AI is already present in health care, financial services, automation, climate change, scientific research, both on the edge as well as the cloud and data center levels. There are many breakthrough developments and innovation in mobility, AI, Smart Robotics, 3D Manufacturing, Smart Homes, Food Sustainability, Digital Assets, Digital TV, Connected Kitchen, 3D Metaverse, Quantum Computing, etc. The world is moving very fast with many new and challenging technologies and concepts for which the energy, power savings and storage are critical. Augmented Reality/Virtual Reality (AR/VR) brings new experiences around the world to our homes and schools.

Advanced thermal management and materials solutions are needed to maintain this fast-paced global technology development. Therefore our critical role as thermal engineers is to look for innovative thermal solutions to address the ever-growing challenges of the current and future technologies. The AI and the overall associated industries will not advance if they are not enabled by the most advanced thermal management solutions. It is with great pride that I see how our thermal engineering roles directly contribute to the growth of technology worldwide. Without advanced cooling, there is no progress ahead on any technology fronts. Cool is in!!! Keep up the great work, and strive for excellence in your activities.

Without you, the ***Electronics Cooling Magazine*** readers and contributors, our role would be greatly diminished. Please keep us posted with your progress as we move forward. We invite you to provide your feedback for our publication content improvement and suggestions for future articles and topics. Please continue to contribute to our publication and publish articles that bring novelty and knowledge to our thermal community, to inspire our young engineers and to spread great thermal management ideas.

Wish you a successful 2023. Stay healthy, happy, inspired and creative!

Victor Chiriac

TECHNICAL EDITORS SPOTLIGHT

Meet the 2023 Editorial Board

VICTOR CHIRIAC, PhD | GLOBAL COOLING TECHNOLOGY GROUP

Associate Technical Editor

A fellow of the American Society of Mechanical Engineers (ASME) since 2014, Dr. Victor Adrian Chiriac is a co-founder and a managing partner with the Global Cooling Technology Group since 2019. He previously held technology/engineering leadership roles with Motorola (1999-2010), Qualcomm (2010 – 2018) and Huawei R&D USA (2018 – 2019). Dr. Chiriac was elected Chair of the ASME K-16 Electronics Cooling Committee and was elected the Arizona and New Mexico IMAPS Chapter President. He is a leading member of the organizing committees of ASME/InterPack, ASME/ IMECE and IEEE/CPMT Itherm Conferences. He holds 21 U.S. issued patents, 2 US Trade Secrets and 1 Defensive Publication (with Motorola), and has published over 110 papers in scientific journals and at conferences.

► vchiriac@gctg-llc.com

GENEVIEVE MARTIN | SIGNIFY

Associate Technical Editor

Genevieve Martin (F) is the R&D manager for thermal & mechanics competence at Signify (former Philips Lighting), The Netherlands. She has worked in the field of cooling of electronics and thermal management for over twenty years in different application fields. From 2016 to 2019, she coordinated the European project Delphi4LED, which dealt with multi-domain compact modeling of LEDs and, since 2021, is coordinating the AI-TWILIGHT project. She served as general chair of the SEMI-THERM conference and is an active reviewer and technical committee member in key conferences including SEMI-THERM, Therminic, and Eurosime. She has over 20 journal and conference papers and 16 worldwide patents.

► genevieve.martin@signify.com

ALEX OCKFEN, P.E. | META

Associate Technical Editor

Alex Ockfen is a simulation engineer at Meta (formerly Facebook), providing technical leadership for thermal and structural design of consumer electronics products. He held previous positions at Raytheon where he obtained experience in thermal management and electronics cooling of a wide range of aerospace and defense applications. He has more than 10 journal and conference publications, is an inventor on multiple patents, is a professional mechanical engineer, and is currently serving as program chair of the SEMI-THERM conference.

► alex.ockfen@fb.com

ROSS WILCOXON | COLLINS AEROSPACE

Associate Technical Editor

Dr. Ross Wilcoxon is a Senior Technical Fellow in the Collins Aerospace Advanced Technology group. He conducts research and supports product development in the areas of component reliability, electronics packaging, and thermal management for communication, processing, displays, and radars. He has more than 40 journal and conference publications and is an inventor on more than 30 US Patents. Prior to joining Rockwell Collins (now Collins Aerospace) in 1998, he was an assistant professor at South Dakota State University.

► ross.wilcoxon@collins.com

COOLING EVENTS

News of Upcoming 2023 Thermal Management Events

MAY
9

ThermalLIVE™ Summit
Online Event in EST

ThermalLIVE Summit is a chance for thermal engineers, researchers, professionals and many more to come together to learn from industry experts on the front lines. With ongoing technology developments, this event is your chance to learn answers to questions and hear industry-leading liquid cooling technical experts' opinions and recommendations.

Desc. source: electronics-cooling.com
► **thermal.live**

MAY
29-31

European Conference of Heat Treatment
Genova, Italy

AIM recently announced the **ECHT 2023 Conference** will be in Genova, Italy, at Magazzini del Cotone, May 29-31, 2023. ECHT 2023 will cover all relevant topics for the heat treatment and surface engineering community. The conference will include a special focus on sustainability. Sustainability, with its three pillars — environmental, economic, and social dimensions — is playing a key role to address ongoing and future challenges. The metallurgical and mechanical industries are leading the way in creating a healthy development model for the environment and for future generations. Presentations and papers from industry, university, and research centers on the topic will encourage the discussion and increase awareness on the matter.

Desc. source: electronics-cooling.com
► **aimnet.it/echt2023.htm**

JUL
3-4

ICEHTFMT 2023
Online Event in CET

International Conference on Experimental Heat Transfer, Fluid Mechanics and Thermodynamics aims to bring together leading academic scientists, researchers and research scholars to exchange and share their experiences and research results on all aspects of Experimental Heat Transfer, Fluid Mechanics and Thermodynamics. It also provides a premier interdisciplinary platform for researchers, practitioners and educators to present and discuss the most recent innovations, trends, and concerns as well as practical challenges encountered and solutions adopted in the fields of Experimental Heat Transfer, Fluid Mechanics and Thermodynamics.

Desc. source: electronics-cooling.com
► **waset.org/experimental-heat-transfer-fluid-mechanics-and-thermodynamics-conference-in-july-2023-in-prague**

Network Implementation of Advective Thermal Conductances

Mark Whittum, P.E.
Senior Principal Mechanical Engineer
Collins Aerospace

Overview

Accurate modeling of thermal networks requires that all relevant modes of heat transfer, including advection, be included. Otherwise, component temperatures may be under- or over-estimated. This article presents a method for systematically including advection in one-dimensional (1D) thermal networks, via the use of unidirectional elements in the thermal network equation. This method can be expanded for use in larger multi-node thermal networks that use Excel, Mathcad, or MATLAB for automated assembly of conductance arrays.

Nomenclature

q	Heat rate (W)
$\dot{m}$	Mass flow rate (kg/s)
C_p	Specific heat (J/kg°C)
T_{out}	Fluid outlet temperature of the duct / heat sink (°C)
T_{in}	Fluid inlet temperature of the duct / heat sink (°C)
K_{adv}	Advective thermal conductance (W/ °C)
n	Number of nodes in a thermal network
T_i	Temperature at node i (°C)
q_i	Heat load at node i (W)
$K_{i,j}$	Conductance between node i and node j (W/°C)
K_{air}	Advective conductance for air at a given mass flow rate (W/°C)
C_{pair}	Specific heat of air (approximately 1000 J/kg°C)

Advection

Accurate modeling of thermal networks requires that we include all relevant modes of heat transfer:

- Conduction – diffusion of heat due to molecular motion
- Radiation – electromagnetic waves
- Convection – heat transfer due to motion of fluid (includes diffusion and advection)
- Advection – heat transfer due to bulk motion of a fluid

Practically speaking, when modeling heat transfer to a fluid (convection), we should include the effects of heating of the fluid itself (advection) in the thermal model. Neglecting advection completely will result in underestimating the temperature rise of a component. Including advection incorrectly will result in erroneous estimation of the temperature rise of a component. The heat transferred via advection to a fluid flowing through a duct or a heat sink is expressed in *Equation 1*:

$$q = \dot{m} \cdot C_p \cdot (T_{out} - T_{in}) \qquad \{1\}$$

Where q is the heat transported by the fluid (W), ṁ is mass flow rate of fluid in a duct (kg/s), C_p is the specific heat of the fluid (J/kg°C), T_{out} is the fluid outlet temperature of the duct (°C), and T_{in} is the fluid inlet temperature of the duct (°C).

Equation 1 can be recast as an advective thermal conductance, in *Equation 2*:

$$K_{adv} = \frac{q}{T_{out} - T_{in}} = \dot{m} \cdot C_p \qquad \{2\}$$

Where K_{adv} is the advective thermal conductance (W/ °C), which is the inverse of the thermal resistance.

Mark Whittum, P.E.
Collins Aerospace
Mark Whittum is a Senior Principal Mechanical Engineer at Collins Aerospace in Westford, MA, and adjunct faculty in the Department of Mechanical Engineering at the University of Massachusetts - Lowell. He is responsible for the design, analysis, and test of thermal management systems for electronics pods and avionics. Prior to joining Collins (then Goodrich) in 2003, he worked for the Kollsman Instrument Company on their line of avionics and cabin pressure control systems.

Options For Modeling Advection

A previous *Electronics Cooling Magazine* article [1] demonstrated multiple methods to model advection in a reduced order thermal model and the level of inaccuracy associated with each method. The least accurate (and simplest) method is to ignore advection and assume a component transfers thermal energy to air at the heat sink (or duct) inlet temperature. The most accurate (and complex) method is to use the ε-NTU method, from heat exchanger analysis techniques. A method with acceptable levels of complexity and accuracy is to assume that the heat is rejected to the "midpoint temperature" of the air, meaning the average of the inlet and exit air temperatures in the sink. Another method from Steinberg [2] is to assume that the heat dissipating component rejects heat to the exit air temperature of the heat sink/duct. This last method is inherently conservative in that the exit air temperature of the sink is always higher than both the surface of the heat sink and the average air temperature in the sink, resulting in predicted component temperatures that are always higher than those predicted by the ε-NTU or midpoint methods. As will be demonstrated by this article, it also has the advantage of being able to be folded easily into a multi-node network thermal model, as long as precautions are taken to properly implement the advection network elements.

Example

The following model demonstrates both the incorrect and the correct ways to implement advective thermal network elements. *Figure 1* depicts a duct formed by two printed circuit boards (PCBs). Air at a temperature T_{in} = +55°C and a mass flow rate of ṁ=0.010kg/s enters the inlet of the PCB slot. The active side of one PCB has two identical components attached to it and each component has an identical heat sink bonded to it. The components are Field Programmable Gate Arrays (FPGAs), each dissipating 15W. The heat sinks each have a conductance K_{sink} = 0.83W/°C (thermal resistance R_{sink} = 1.2°C/W) for the flow rate used in this example.

Figure 1

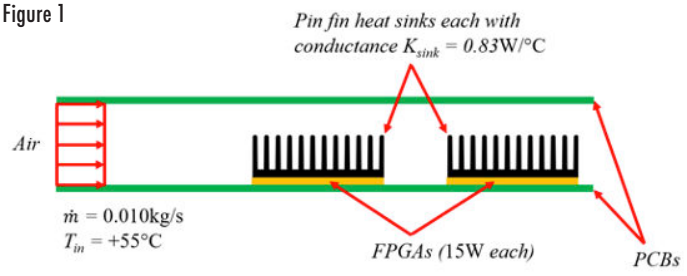

Using the "exit temperature" advection approach described in the previous section, the calculation of component and air temperatures can be performed as follows:

1) The 0.010 kg/s of inlet air at +55°C is heated to +56.5°C by the first 15W component:

   15W / 10.0W/°C + 55.0°C = +56.5°C

2) The front 15W component dissipates heat via convection to +56.5°C air, resulting in a front heat sink temperature of +74.6°C:

   15W / 0.83W/°C + 56.5°C = +74.6°C

3) The air downstream of the front component at +56.5°C is heated to +58.0°C by the rear 15W component:

   15W / 10.0W/°C + 56.5°C = +58.0°C

4) The rear 15W component dissipates heat via convection to +58°C air, resulting in a rear heat sink surface temperature of +76.1°C:

   15W / 0.83W/°C + 58.0°C = +76.1°C

Even though the ε-NTU method would yield the "exact" solution, for purposes of this discussion the preceding results will be referred to as the "correct" results since the intent is that the heat from a component is convected to the exit temperature of the heat sink or duct.

Thermal Network – Initial

The compact equation for calculating the temperatures in a thermal network can be seen in *Equation 2*:

$$T_i = \frac{q_i + \sum_{j=1}^{n} K_{i,j} T_j}{\sum_{j=1}^{n} K_{i,j}} \qquad \{3\}$$

Where n is the number of nodes in the network, T_i is the temperature at node i (°C), q_i is the heat load at node i (W), and $K_{i,j}$ is the conductance between node i and node j (W/°C). Using this relationship, the example in the previous section can be set up as a thermal network problem as shown in *Figure 2*, and the nodal temperatures. Elements 1 and 2 are advective conductors with a value of K_{air}, which is calculated using *Equation 2*:

$$K_{air} = \dot{m} \cdot C_{p,air} \qquad \{4\}$$

Since the mass flow rate ṁ=0.010kg/s and the specific heat of air Cp_{air} = 1000J/kg°C, the value for K_{air} is determined to be 10W/°C.

Figure 2

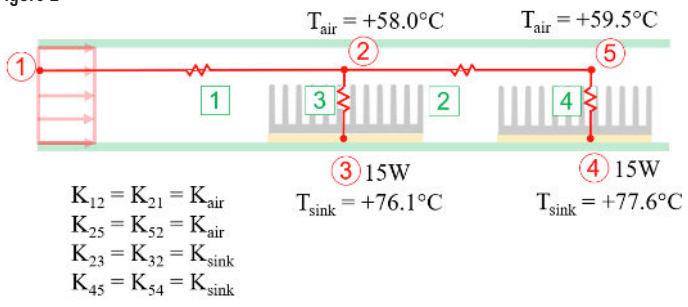

Note that all the conductive elements in the model shown in *Fig-*

ure 2 are bilateral, meaning that they can conduct heat in either direction. Note also that the calculated component temperatures do not match the results from the "correct" solution. The network model returns a value of +76.1°C, where the "correct" solution was +74.6°C. Likewise, the network model returns a value of +77.6°C, for the second heat sink, where the "correct" solution was +76.1°C. The issue lies with the modeling of the advective conductors. For the heat sink conductors, thermal energy can flow either from a hot sink to cooler air, or from warmer air to a cooler sink. In the advective element the heat can only flow in one direction: in the direction of the fluid flow. Heat can't flow upstream in the fluid from the duct exit to the entrance. The question is: how to model this in a thermal network?

Thermal Network – Final

The way to achieve the correct solution in the thermal network model is by modeling the convection conductors as unidirectional, i.e., only able to pass heat in one direction. *Figure 3* shows the advection conductors as diodes, which can only pass heat from the hot downstream node to the cooler upstream node,

Figure 3

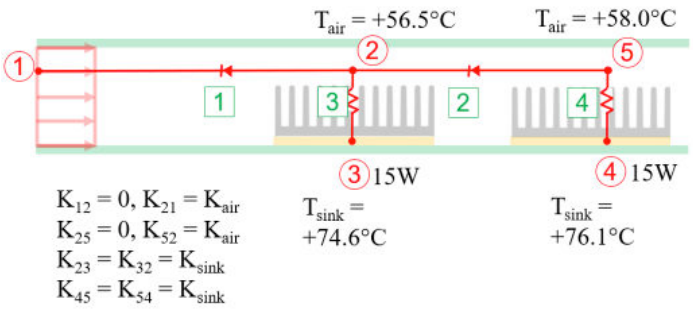

instead of resistors. Note that the diode direction is counterintuitive, in that it is opposite the direction of fluid flow. If the advective node numbering scheme is that the i node is upstream and the j node is downstream, $K_{i,j}$ is always 0 and $K_{j,i}$ is the K_{air} advective conductance calculated previously. When the advective conductor is rendered unilateral in this way, which prevents heat from flowing from the cooler upstream node to the hotter downstream node, the correct temperature results are achieved.

Table 1: Excel Implementation of Unidirectional Advection Conductors

INPUTS			
T_inlet	*55*	*degC*	*MIL5400 temperature at SL*
mdot_slot	*0.01*	*kg/s*	*Sink mass flow rate*
Cp_air	*1000*	*J/kg*degC*	*Specific heat of air*
K_air	*=mdot_slot*Cp_air*	*W/degC*	*Advective conductance*
K_sink	*0.83*	*W/degC*	*Convective conductance of heat sink*
CONDUCTORS			
K_12	*0*	*W/degC*	*Advective conductance (0 in direction of flow)*
K_21	*=K_air*	*W/degC*	*Advective conductance*
K_23	*=K_sink*	*W/degC*	*Convective conductance of 1st heat sink*
K_32	*=K_sink*	*W/degC*	*Convective conductance of 1st heat sink*
K_25	*0*	*W/degC*	*Advective conductance (0 in direction of flow)*
K_52	*=K_air*	*W/degC*	*Advective conductance*
K_45	*=K_sink*	*W/degC*	*Convective conductance of 2nd heat sink*
K_54	*=K_sink*	*W/degC*	*Convective conductance of 2nd heat sink*
NODAL HEAT LOADS			
Q_3	*15*	*W*	*1st FPGA dissipation*
Q_4	*15*	*W*	*2nd FPGA dissipation*
NODAL TEMPERATURES			
T_1	*=T_inlet*	*degC*	*Inlet - fixed*
T_2	*=(K_21*T_1+K_23*T_3+K_25*T_5)/ (K_21+ K_23+K_25)*	*degC*	*mid-slot air temp*
T_3	*=(Q_3+K_32*T_2)/K_32*	*degC*	*Sink 1 temp*
T_4	*=(Q_4+K_45*T_5)/K_45*	*degC*	*Sink 2 temp*
T_5	*=(K_52*T_2+K_54*T_4)/ (K_52+K_54)*	*degC*	*outlet temp*

An Excel implementation of the preceding is shown in *Table 1* (on the previous page), with formulas instead of values shown. For Excel implementation, iterative calculations must be enabled. Variables do not need to be named fields; this is only done here for clarity.

Discussion

The power of this methodology becomes even more apparent when used in conjunction with more sophisticated array management schemes in Excel, which permit automated assembly of the conductivity array and solution of the thermal network equation for each node. The output area of one such Excel sheet is shown below in *Table 2*.

The Excel sheet depicted in *Table 2* has the capacity for only 20 nodes and 20 conductors, which is sufficient for a typical reduced order thermal network model. The model shown is set up starting with a connectivity array (1) of elements and nodes. A conductivity array is generated by using Excel's INDEX and IF functions from the conductances (2) taking into account the unidirectional nature of advection elements. The elements of the conductivity array are then multiplied by the nodal temperature array to create a conductivity-temperature array (4). Boundary conditions and loads are input (5). Combining (3), (4), and (5), the thermal network relationship (*Equation 2*) is formed, and the nodal temperature results generated (6). The advantage of a sheet such as that shown in *Table 2* is that it can be made more generic, used for multiple different models, and distributed among multiple analysts for use and refinement.

Note that a matrix-based solution approach, such as that used in [3],[4] does not work correctly with unidirectional advection conductors because the resulting conductance matrix is not symmetric, and therefore not invertible.

Summary

This article described an approach for systematically including advective conductances in a thermal network model. The method allows multiple flow-path segments and heat dissipators. The conductors that account for advection resistance are unidirectional, which prevents the mathematical possibility of heat flowing from the exit of the duct to the entrance of the duct. Since the heat dissipators are linked in the network to the exit node of the duct, the temperatures predicted are higher than that which would be predicted by the ε-NTU method and are therefore conservative. This method can be implemented in Excel, Mathcad, MATLAB, or any coding package that will allow automated assembly of the conductance array.

Table 2: Excel Sheet for Generating Conductance Array Automatically with Unidirectional Advection Conductors

Connectivity input and element results

Input Connectivity			Input Description	Conductance	T_from	T_to	Q_elem
Conductor Number	From node	To node		W/K	degC	degC	W
elem	node_i	node_j	Description	K_ij	T_i	T_j	Q_ij
1	1	2	inlet air	1.00E+01	55.00	56.50	-1.50E+01
2	2	3	1st FPGA	8.30E-01	56.50	74.57	-1.50E+01
3	2	5	outlet air	1.00E+01	56.50	58.00	-1.50E+01
4	4	5	2nd FPGA	8.30E-01	76.07	58.00	1.50E+01
5	5	1	outlet air to amb	1.00E+01	58.00	55.00	3.00E+01

Nodal constraint input and nodal results

Node	1	2	3	4	5
Input name	Air in	Air mid	FPGA 1	FPGA 2	Air out
Input power			15W	15W	
Input fixed temperature	55.0C				
T_nodal	55.0	56.5	74.6	76.1	58.0

CONDUCTIVITY ARRAY

Node / Elem	1	2	3	4	5
1		1.00E+01			
2		8.30E-01	8.30E-01		
3					1.00E+01
4				8.30E-01	8.30E-01
5	1.00E+01				
Sum	1.00E+01	1.08E+01	8.30E-01	8.30E-01	1.08E+01

CONDUCTIVITY x TEMP ARRAY

Node / Elem	1	2	3	4	5
1		550.0			
2		61.9	46.9		
3					566.0
4				48.1	63.1
5	580.0				
Sum	580.00	611.90	46.90	48.14	628.14
T_final	55.0	56.5	74.6	76.1	58.0

References

[1] Ross Wilcoxon, "Advective Thermal Resistance", Electronics Cooling Magazine, Summer 2022, pp. 6-8

[2] Dave S. Steinberg, "Cooling Techniques for Electronic Equipment", 2nd Edition, Wiley, 1992

[3] Ross Wilcoxon, "A Spreadsheet Based Matrix Solution for a Thermal Resistance Network: Part 1", Electronics Cooling Magazine, September, 2010

[4] Ross Wilcoxon, "A Spreadsheet Based Matrix Solution for a Thermal Resistance Network: Part 2", Electronics Cooling Magazine, June, 2011

The World's Largest, Online Thermal Management Event

ONLINE EVENT

MAY 9, 2023

The Thermal LIVE Summit Experience

Thermal LIVE Summit is a free, online event for electronics and mechanical engineers in the thermal management space to learn about the latest innovations, trends, and challenges directly from industry thought leaders. Topics include best practices in thermal design, next generation substrates, optimization of EV power control units, product demonstrations, and more.

Join us live on May 9 or register to view on demand at your convenience. See you there!

thermal LIVE™ SUMMIT

Generative Design and Advanced 3D Printing: A Copper CPU Cooler with 55% Lower Thermal Resistance

Sarah da Silva Andrade, Niels Verdijck, Lieven Vervecken
Diabatix

Suraj Dinkar Jadhav
Principal Materials Engineer at Amanovis

Introduction

Effective cooling is essential for CPUs, as they generate significant heat during operation while being very temperature sensitive. Improved cooling allows for maintaining the functionality of high-performance computer hardware. In this article, we demonstrate a unique approach to improving the cooling of high-performance components by combining thermal and flow-based topology optimization methodology with additive manufacturing of highly conductive copper, with experimental validation of the results.

Generative Design: The Key To An Optimal Heatsink

Generative design uses Artificial Intelligence (AI) technology to generate one or multiple designs, starting only from system requirements, such as materials, boundary conditions, objectives, and constraints. Different techniques exist to gather and process information from subsequent design iterations. A popular strategy uses topology optimization. Contrary to traditional design methods, such as parametric and shape optimization, topological optimization does not require an initial design input, only the

Sarah da Silva Andrade
Ms. Andrade is the Marketing Engineer at Diabatix, a software company specialized in advanced thermal design. She holds a B.Sc. and M.Sc. in Civil Engineering from the University of Campinas in Brazil, awarded in 2016 and 2019. Prior to her role at Diabatix, Ms. Andrade worked as a research assistant in the Civil Engineering Department at KU Leuven.

Dr. Suraj Dinkar Jadhav
Dr. Jadhav is a Principal Materials Engineer at Amanovis, a startup in Belgium that manufactures high-tech and quality-critical metallic parts using additive manufacturing processes. He did his Ph.D. (2016-2021) and master's (2014-2016) in Materials Engineering at KU Leuven. Dr. Jadhav obtained the Ph.D. degree with a Summa cum laude grade and congratulations of the board of examiners. Prior to his master's, he completed his bachelor's education in Metallurgical Engineering from the College of Engineering Pune, India (2006-2010) and worked as a Materials Lab Engineer in the R&D center of Bekaert India (2010-2014).

Niels Verdijck
Ir. Verdijck joined Diabatix team on July 2021, after achieving his master's degree in mechanical engineering at the renowned KU Leuven. During his time at the University, Ir. Verdijck worked on multi-objective topology optimization of a microjet cooler. Currently, as Customer Support Engineer, he focuses on helping ColdStream users with their projects by providing them with insights and feedback.

Dr. Lieven Vervecken
Dr. Vervecken is the CEO and co-founder of Diabatix, a software company specialized in advanced thermal design. Prior to founding Diabatix, Dr. Vervecken received a Ph.D. in mechanical engineering from the renowned KU Leuven in the field of numerical simulations. Dr. Vervecken incorporated his expertise into the advanced A.I. technology at the heart of Diabatix. What started as a small venture has become a fast-growing SaaS company serving multinationals worldwide. Dr. Vervecken is the lead author of multiple peer-reviewed journal articles and an experienced keynote speaker at national and international conferences.

definition of a design space.

In this case study, generative design was applied to optimize the cooling channels in a CPU cooler. By minimizing a cost objective and meeting operational and manufacturing constraints, the process generated an ideal solid structure within a fluid, seeking the most efficient material distribution in accordance with the design objectives.

Copper: An Attractive Material For Heat Sink

Copper's high thermal conductivity (398 W/m K)) makes it an interesting material for 3D printing of thermal management components. However, its high reflectivity for conventionally employed infrared lasers (wavelength of 1070 nm) limits the absorption of the laser light for melting. Furthermore, its high thermal conductivity quickly dissipates the energy absorbed by the laser, which creates challenges in producing copper components with laser-based 3D printing technologies.

Several strategies are employed in the industry to tackle these issues. In this study, the approach of using laser-absorptive copper powders was chosen. This method has three benefits: (i) material can be melted in conduction mode with higher build rates, while the smaller deep melt pool dimensions lead to excellent print resolution, (ii) standard L-PBF (Laser Powder Bed Fusion) equipment, with reliable and high beam-quality infrared lasers, can be used, and (iii) laser absorptive powders have excellent flowability and oxidation-resistant properties. These allow printed copper components to be produced in a broad and stable processing environment.

In addition to conductivity, material yield strength and specific weight are important when designing complex-shaped thermal management components with fine features [1,2].

The primary advantages of this approach are (i) the full density and a good combination of conductivity and strength: tensile strength up to 630 MPa, yield strength up to 510 MPa, ductility up to 30%, electrical conductivity up to 90% IACS, and thermal conductivity up to 360 W/(m K) for CuCr1Zr material; (ii) the ability to form thin-walled and complex-shaped structures with thickness down to 200 μm; (iii) the broad processing window allows repeatable and reproducible build quality; (iv) final part properties can be tailored to an application; and (v) the approach works with a 400 W laser that does not overheat the baseplate and powder, which improves powder recyclability.

Modeling the CPU Cooling System

A liquid CPU cooler typically consists of one or multiple solid parts and a liquid coolant. Simulation of this type of system is known as a Conjugate Heat Transfer (CHT) problem. The Navier-Stokes equations [3], consisting of expressions for the conservation of mass, momentum, and energy, are solved in the fluid domain. Closure of the momentum equation is provided by applying turbulence models to compute the turbulent viscosity. Various turbulence models exist; RANS, which is the most widely used for wall-bounded flows, was used for this case study.

For the solid region, only conservation of energy applies [4]:

$$\rho c_p \frac{\partial T}{\partial t} - \nabla \cdot \kappa \nabla T = Q$$

where ρ, c_p, κ and T are the material density, specific heat, thermal conductivity, and temperature, while Q refers to the heat source.

Heat transfer between the solid and the fluid depends only on the local physical properties and the temperature difference between the respective cells adjacent to the wall. At this wall interface, equilibrium conditions are imposed, which dictates continuous heat flux and temperature over the interface. While computationally expensive, this approach provides detailed insight into the physics of the problem, which gives the optimizer a more realistic characterization of each design. This is fundamental to accurately exploring the design space and eventually finding an optimal design.

Defining the Optimization Problem

The objective/constraint formulation is a common method for defining and solving optimization problems. In this approach, an objective function expresses the goal of the optimization problem, which is subject to constraints that limit the solutions to those that satisfy certain conditions:

$$minimize\ J$$

$$subject\ to: \quad X \leq C$$

In the iterative design process, calculations are performed using adjoint equations to determine the sensitivity of the objective function to each system variable and to compute gradients for optimization. Examples of objectives are minimizing temperature or weight, while examples of constraints are a maximum allowable pressure drop or any manufacturing-related limitations.

CPU Cooler: Comparative Case Study

The case study compares a commercially available skived fin heat sink with one using a generative design using the same materials, operating conditions, boundary conditions, and outer envelope for both models. The base plate has dimensions 60.0 × 59.9 mm^2 (*Fig. 1a*). The material of the heat sink is the copper used for L-PBF with ρ = 8910 kg/m^3, c_p = 370 J/(K kg) and κ = 360 W/(m K).

The coolant is a 40/60 mixture of water and ethylene glycol with ρ = 1050 kg/m^3, the dynamic viscosity of μ = 0.00178 Pa s, c_p= 3220 J/(K kg), and κ = 0.376 W/(m K). The inlet flow rate was fixed at 0.82 L/min and T = 313.15K (40°C). *Fig. 1a* shows the inlet and outlet locations of the coolant.

Figure 1. CPU Heat Sink

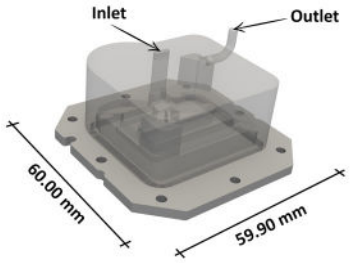

Figure 1a. Top view: dimensions, inlet and outlet locations

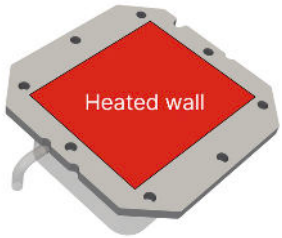

Figure 1b. Bottom view: heated wall

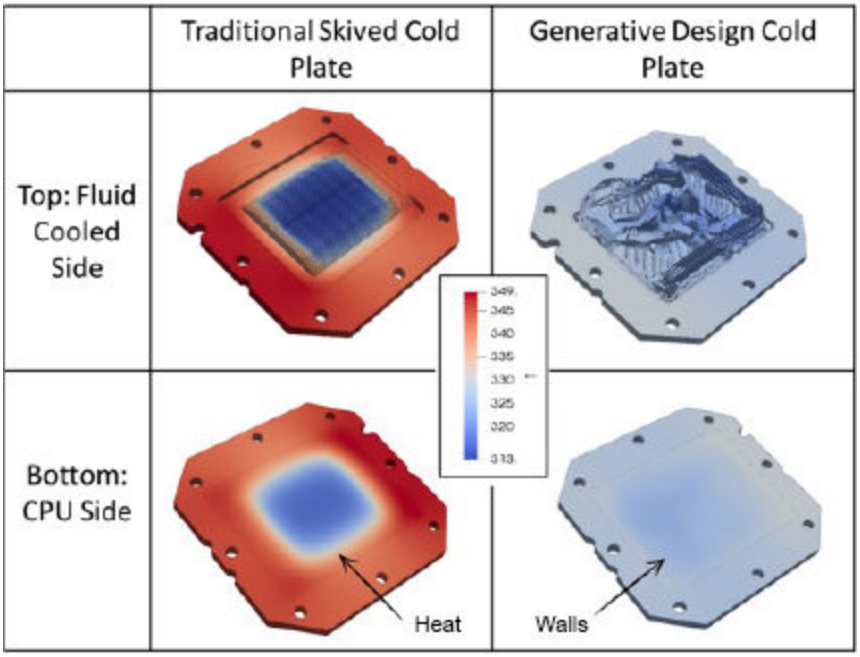

Figure 2. Temperature field (top and bottom view) in K of the skived fin and the generative design heat sinks

The modeled heated wall (*Fig. 1b*) was an Intel 1700 that uniformly dissipated Q = 250 W over the contact area between the CPU and the heat sink.

Traditional design

The simulated temperatures of the skived fin copper heat sink are shown in *Fig. 2* for the liquid-cooled side and the surface attached to the CPU. The traditional design shows a maximum temperature of 349.3K (76.1°C), with the system cooling it down to 316.2K (43.0°C). The temperature variance of the contact surface between the heat source and the heat sink is 124.6 K^2 and the pressure drop was 11 kPa.

Generative design

The generative design utilizes targets and constraints to develop an optimized model. The target for the design was minimizing the temperature of the heated surface. This goal function reduced the temperature across an element by focusing on the highest temperatures:

$$J = \int_S T \, \mathrm{d}S$$

where J is the value of the objective in K, T is the temperature distribution on a boundary in K, and S is the surface of the boundary where the objective is calculated in m^2.

The inlet is constrained to a static pressure drop in the flow through the heat sink that is less than or equal to the prescribed value:

$$\int_A p \, \mathrm{d}A \leq \Delta p$$

where p is the actual pressure at the inlet, and Δp is the allowable pressure drop, set as Δp = 11 kPa.

Fig. 3 shows the final generative design for the CPU cooler setup. The natural freeform shape combines large and small channels without symmetry.

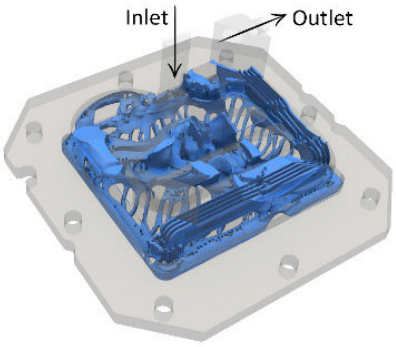

Figure 3. Generative design of the CPU cooler

The simulation results for the generative-designed heat sink are shown in *Fig. 2* for the liquid-cooled and heated sides. The temperature on the heated wall ranges from 323.4K (50.3°C) to 329.6K (56.4°C), and its variance is 2.4 K^2.

The design region was modeled with 17M design variables. The full optimization loop and the CFD analyses were run in parallel on 256 CPUs.

Discussion

To compare the heat sink performance, the thermal improvement

is calculated using the thermal resistances of each of the models:

$$R_{\text{th}} = \frac{T_{\text{max}} - T_{\text{in}}}{Q}$$

where T_{max} is the maximum temperature on the heat source and T_{inlet} is the inlet fluid temperature.

The thermal resistance of the skived heat sink was 0.145 K/W, while the resistance of the generative design model was 0.066 K/W - a 54.5% lower thermal resistance.

In addition, the temperature range is about 33K for the skived heat sink and only 6K for the optimized design. Although not explicitly imposed as a target, a uniform temperature is important to ensure uniform thermal degradation over the chip.

The difference in temperature variances on the heated source (CPU) is visible in *Fig. 2*. The more uniform temperature in the generative design model is due to the distribution of the cooling channels along the total area of the heated source (*Fig. 3*). The skived fin heat sink occupies a smaller area when compared to the heated source, which reduces the fluid flow pressure drop at the expense of less uniform CPU cooling.

Experimental Validation

An experimental study was carried out to validate the results of the optimized CPU cooler. Due to laboratory testing constraints, test boundary conditions could not match simulation conditions. Therefore, new numerical simulations with updated materials and operating conditions matched the experimental test conditions (*Fig. 4*) were made.

As mentioned, manufacturability was treated as a design constraint when defining the design region to ensure the design could be 3D printed; the resulting device is displayed in *Fig. 5*.

The top and bottom housings were fabricated in thermoset epoxy, with the following properties: ρ = 1150 kg/m^3, c_p = 1100 J/(kg K) and κ = 0.17 W/(m K). The heat sink material is L-PBF copper, with the properties already described. The main differences between the test and design configurations were the coolant and the heating system. Deionized water, with ρ = 998 kg/m^3, c_p = 4182 J/(kg K), κ = 0.598 W/(m K) and μ = 0.001002 Pa s, was used as the liquid coolant. The system received 22.5 W of heat to represent the chip, modeled as silicon nitride (ρ = 3210 kg/m^3, c_p = 750 J/(kg K) and κ = 40 W/(m K)), and the heat was spread with a copper patch (ρ = 8960 kg/m^3, c_p = 385 J/(kg K) and κ = 386 W/(m K)).

The heat sink's performance ($\Delta T = T_{max,heater} - T_{inlet,coolant}$), including uncertainty, is shown for flow rates ranging from 75 to 200 ml/min in *Fig. 6*. The experimental data corroborates the simulated values within the uncertainty interval, showing a very good agreement between them.

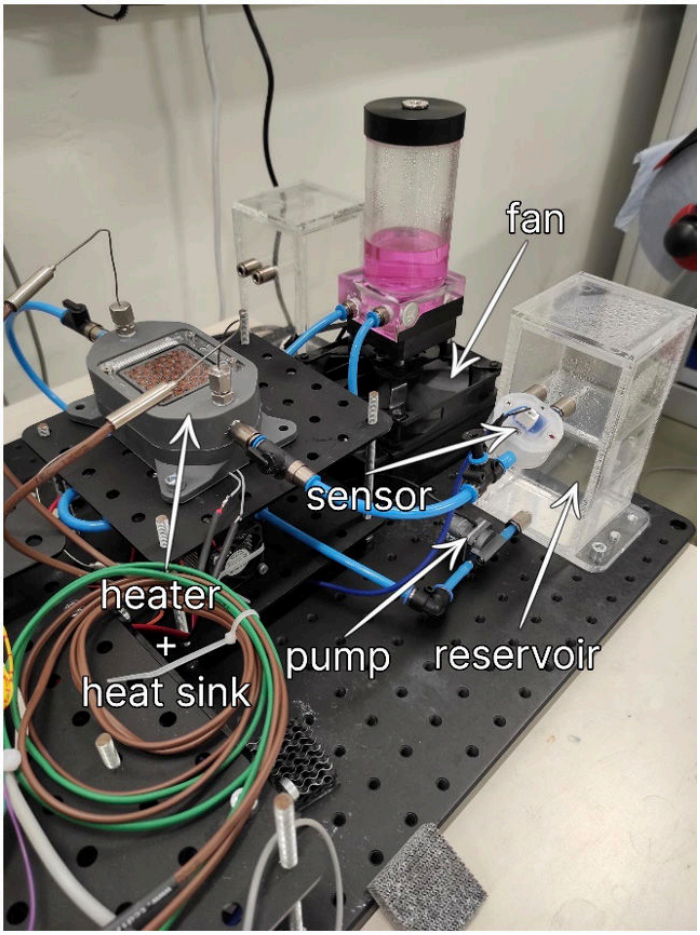

Figure 4. Experimental Setup

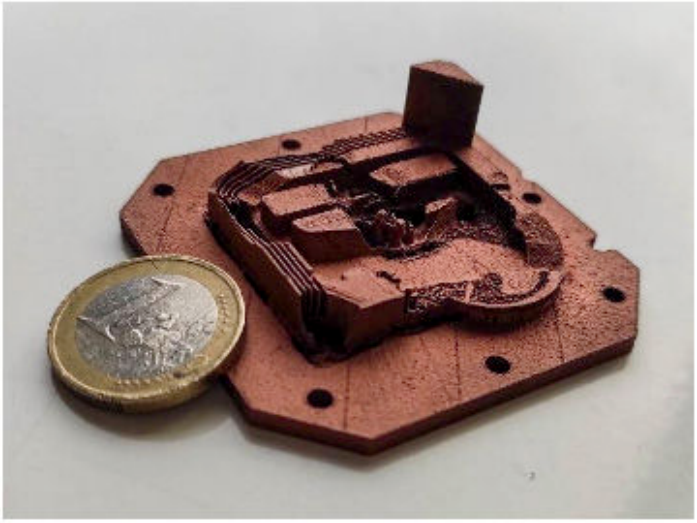

Figure 5. 3D printed generative CPU cooler design model

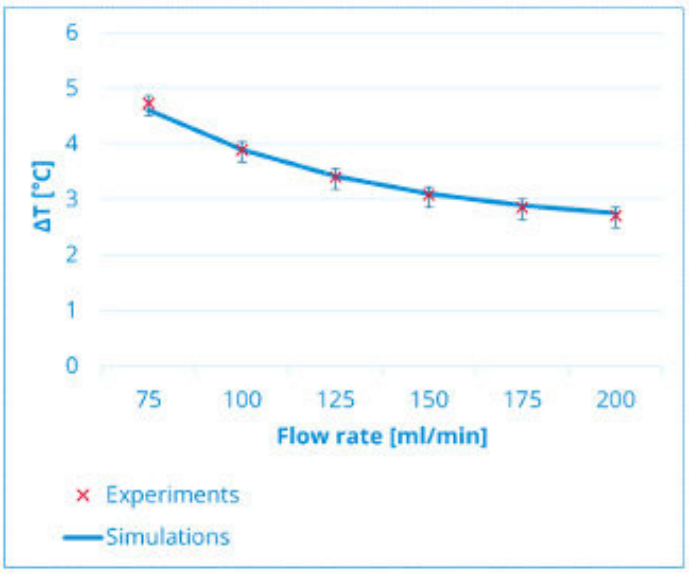

Figure 6. Experimental validation results

It must be stressed that 3D printing is not required for generative design. Other methods, such as milling and die casting, can be adopted by applying the manufacturing constraints.

Conclusion

The value of the generative thermal design process was illustrated through the design of a CPU cooler. The methodology autonomously suggests cooling system geometries in natural freeform shapes to reach an optimized design. The performance of a generatively designed heat sink was compared to a commercial copper skived fin design. The thermal resistance was improved by 55% in the generative design CPU cooler, which also greatly reduced heat source temperature variance. Experimental results matched simulations, showing that generative design offers a way to break new ground in thermal design.

Acknowledgments

Experts from Diabatix and Amnovis conducted this study. The generative design and the CFD simulations were performed using ColdStream by Diabatix [5] and 3D-printed by Amnovis [6]. KU Leuven performed the experimental tests.

References

[1] Jadhav, S.D. et al, 2019. Influence of carbon nanoparticle addition (and impurities) on selective laser melting of pure copper. Materials, 12(15), p.2469.
[2] Jadhav, S.D. et al, 2020. Mechanical and electrical properties of selective laser-melted parts produced from surface-oxidized copper powder. Material Design & Processing Communications, 2(2), p.e94.
[3] C. Hirsch, 2007. Numerical computation of internal and external flows: The fundamentals of computational fluid dynamics. Elsevier.
[4] K. Shea, R. Aish, and M. Gourtovaia, 2005. "Towards integrated performance-driven generative design tools". In: Automation in Construction 14.2, pp. 253–264.
[5] https://coldstream.diabatix.com.
[6] https://www.amnovis.com/copper-lpbf.

Guide to Simulation of Vapor Chambers as Anisotropic Conduction Heat Spreaders

Kalind Baraya, Justin A. Weibel, Suresh V. Garimella
School of Mechanical Engineering, Purdue University

Introduction

Vapor chambers are passive two-phase devices used to spread heat from localized hotspots to larger surface areas. The device utilizes the latent heat of evaporation of an internal fluid to passively transport heat from the evaporator (heat source) to the condenser (heat sink) across very low temperature drops. Condensed liquid returns to the evaporator from the condenser via capillary pumping by an internal wick. Due to the mass, momentum, and energy transfer coupling via phase-change processes at interfaces between the wick and vapor core, direct numerical simulation of vapor chamber transport [1–3] is a computationally expensive and complex endeavor. It is therefore of interest for thermal designers to have access to more simplified methods of representing vapor chambers in numerical transport simulations that predict thermal performance without a significant compromise in accuracy.

Effective Representation of a Vapor Chamber as an Anisotropic Material

As an alternative to direct simulation of the internal flow dynamics, vapor chamber thermal transport can be predicted by treating the vapor core as a thermal conduction block with appropriately assigned effective thermal properties (conductivity and specific heat). These effective properties must be chosen to accurately

Kalind Baraya
Kalind Baraya received the B.Tech. degree in mechanical engineering from IIT Guwahati, Guwahati, India, in 2016. He is a currently a Ph.D. Student under the advisement of Dr. Justin A. Weibel and Dr. Suresh V. Garimella at the Cooling Technologies Research Center, School of Mechanical Engineering, Purdue University, West Lafayette, IN, USA. His research focuses on modeling and experimental characterization of vapor chambers and heat pipes, with emphasis on designing vapor chambers operating under steady-state, transient, and dryout-recovery conditions.

Justin A. Weibel
Justin A. Weibel is an Associate Professor in the School of Mechanical Engineering at Purdue University and Director of the Cooling Technologies Research Center (CTRC), a graduated NSF I/UCRC. He received his BMSE in 2007 and PhD in 2012 from Purdue University, West Lafayette, IN, USA. Dr. Weibel's research explores methodologies for prediction and control of heat transport to enhance the performance and efficiency of thermal management technologies and energy transfer processes. He has supervised over 30 Ph.D. and M.S. students and coauthored over 190 referred journal and conference articles. He has been recognized as an Outstanding Engineering Teacher and Outstanding Faculty Mentor in the College of Engineering at Purdue University. He received the 2020 ASME EPPD Young Engineer Award and 2021 ASME K-16 Outstanding Early Faculty Career in Thermal Management Award. Corresponding author, E-mail address: jaweibel@purdue.edu

Suresh V. Garimella
Suresh V. Garimella is currently the President of The University of Vermont (UVM), Burlington, VT, USA, a Professor with the Department of Mechanical Engineering, UVM, and a Distinguished Professor Emeritus of Mechanical Engineering, Purdue University, West Lafayette, IN, USA, where he is the Founder of the National Science Foundation Cooling Technologies Research Center. He has supervised over 90 Ph.D. and M.S. students. He has coauthored over 525 refereed journal and conference publications, and holds 13 patents. The 28 alumni from his research group are now faculty members at prestigious universities around the world. His research group has made seminal contributions to microscale and nanoscale thermal and fluidic engineering, novel materials for thermal management, materials processing and manufacturing, and renewable energy. Dr. Garimella is a member of the National Science Board (NSB) and a Fellow of the National Academy of Inventors, AAAS, and ASME. His contributions to thermal management have been recognized with the 2016 ITherm Achievement Award, the 2010 Heat Transfer Memorial Award, and the 2009 Allan Kraus Thermal Management Medal.

represent the underlying vapor flow dynamics and temperature drops. Vapor chambers are known to have inherently anisotropic heat spreading behavior. A seminal formulation for the effective in-plane thermal conductivity of a vapor chamber based on the vapor core saturation temperature drop was given by Prasher [4]:

$$k_x = k_y = \frac{h_{fg}^2 P \rho h_{vap}^2}{12 R \mu \overline{T}_{sat}^2}, \qquad (1)$$

where h_{fg} is the latent heat of vaporization, P is the vapor pressure, ρ vapor density, h_{vap} is the vapor core thickness, R is the specific vapor gas constant, μ is the vapor viscosity, and $\overline{T}_{sat}$ is the average vapor core saturation temperature. It is important to note that *Equation (1)* has a strong temperature/pressure dependence as it is not an intrinsic material thermal conductivity, and hence the vapor properties (h_{fg}, ρ and μ) and P are calculated at $\overline{T}_{sat}$. Because $\overline{T}_{sat}$ is not known *a priori*, $\overline{T}_{sat}$ is a good initial guess of the vapor chamber condenser temperature.

An alternative formulation is required for the effective cross-plane thermal conductivity of the vapor core. We caution against assuming that the vapor core can be represented as an isotropic material, as use of *Equation (1)* as the effective cross-plane thermal conductivity leads to erroneous temperature predictions [5]. Similarly, the vapor (gas) material thermal conductivity is not an acceptable alternative for the cross-plane thermal conductivity. A more accurate physical representation of the anisotropic nature of vapor core transport was developed in our recent work [5] by comparing the vapor core transport equation to a heat diffusion equation. Effective properties are thereby derived to ensure that, if the vapor core is treated as an anisotropic solid conduction block, the transient and steady-state temperature response would be the same as if directly solving the vapor transport equations [3]. This leads to the same expression for in-plane thermal conductivity as in *Equation (1)* and a new expression for the cross-plane thermal conductance per unit length:

$$k_z = \frac{\phi h_{fg} h_{vap}}{2}, \qquad (2)$$

$$\text{where } \phi = \frac{2\sigma}{2-\sigma} \frac{h_{fg}\rho}{\overline{T}_{sat}^{1.5}} \left(\frac{1}{2\pi R} \right)^{0.5}$$

and σ is the accommodation coefficient while the rest of the nomenclature is the same as for *Equation (1)*. Note that *Equation (2)* is not an intrinsic material thermal conductivity, but rather is a function of vapor thermophysical properties and vapor core thickness. Similar to *Equation (1)*, the vapor properties in *Equation (2)* should be calculated at $\overline{T}_{sat}$. For accurate transient predictions, the effective thermal capacity of the vapor core can be modeled by taking effective density and specific heat properties that are equal to that of the vapor (gas) thermophysical properties as

$$\rho_{eff} = \rho;\ C_{p,eff} = C_p, \qquad (3)$$

where ρ is the vapor density and C_p is the vapor specific heat calculated at $\overline{T}_{sat}$.

Details of the derivation of these effective parameters are available in Ref. [5]. Extensive verification has also been conducted to ensure that using these effective anisotropic vapor core properties in numerical simulations results in the same thermal predictions as an experimentally validated vapor chamber model [3] over a range of cases. The reader is also encouraged to refer to Ref. [5] for details regarding estimates of the error associated with using these parameters that is associated with necessary simplifying assumptions that neglect convective vapor transport (only diffusive transport is considered) and linearization of the Clausius–Clapeyron equation. Lastly, we note that vapor chamber operation is subject to several transport limits, such as the capillary limit, which must be calculated separately; these effective anisotropic properties apply to operation below all such limiting conditions.

Implementation in Numerical Conduction Solvers

Proper implementation of the effective anisotropic conduction parameters given by *Equations (1-3)* into commercial numerical conduction solvers requires care. This is due to the nature of the cross-plane parameter being a conductance per unit length rather than a simple analog for material thermal conductivity. In addition to assigning the correct anisotropic properties, *the vapor core must be meshed with a single element across its thickness*. This ensures that only a single computational node exists along the thickness of the vapor core at a given in-plane location, and allows for solving a cross-plane-averaged temperature at each cell in the vapor core as assumed in the derivation of the effective anisotropic properties. Using more than one computational node across the thickness of the vapor core will lead to an erroneous prediction. The vapor core must be sandwiched between material layers that represent conduction in the wick and the wall of the vapor chamber. These layers can be assigned the correct thermophysical properties (conductivity, density, and specific heat) and are typically assumed to be isotropic.

This guide does not cover calculation of the effective properties of porous wick structures, but readers are directed to Ref. [6], which offers simple expressions to calculate wick thermal conductivity as a function of the wick porosity and geometric parameters.

The following section provides an example implementation of these effective anisotropic properties into a numerical conduction solver. The example considers a specific thermal analysis software tool (Icepak), but the approach is translatable to any fi-

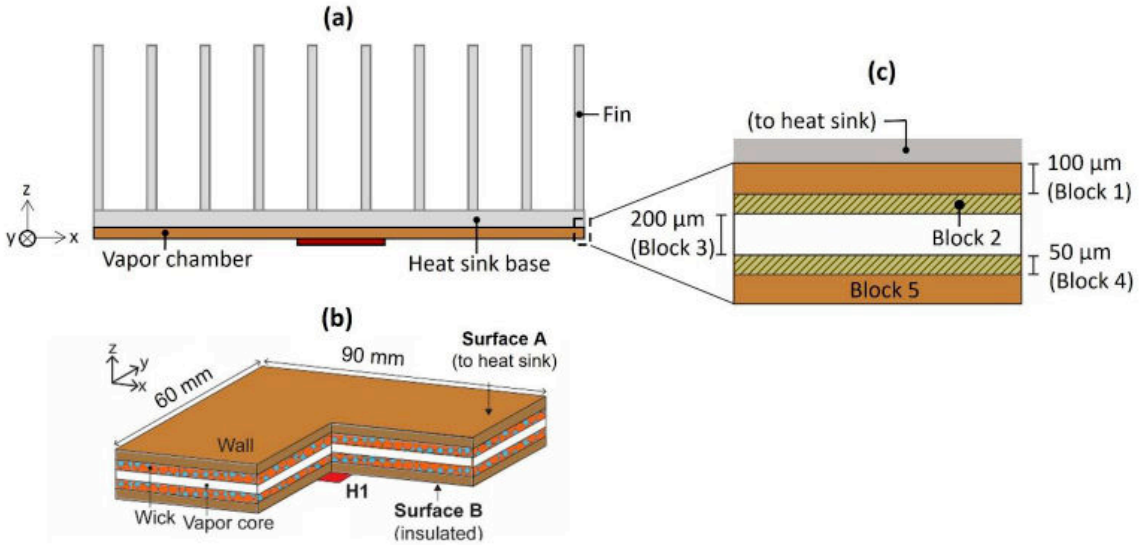

Figure 1. (a) Schematic diagram of the sub-assembly modeled in Ansys ICEPAK. The schematic shows a vapor chamber with a heat sink attached on top. The heat sink is cooled by 3 fans (not shown in the schematic) each with volumetric flow rate of 20 CFM in the y direction. (b) Cut-away view of the vapor chamber with heat source location for the sub-assembly in (a). (c) Cross-sectional view of the model vapor chamber. Note that the figures are not drawn to scale.

nite-volume numerical conduction solver that allows controlled generation of the single-cell-thick vapor core mesh and custom assignment of anisotropic properties.

Demonstration Case

Geometry, model setup, and boundary conditions

Figure 1(a) shows the vapor chamber and heat sink assembly that is considered for demonstrating the implementation of the effective anisotropic properties approach to simulate vapor chamber thermal transport. A heat sink is attached to the top surface of the vapor chamber, both having a 90 mm × 60 mm footprint. *Table 1* summarizes the heat sink design as modeled using the "Heat Sink" tool in ANSYS Icepak. The heat sink is cooled by three fans (20 CFM each at 20°C ambient temperature) specified using the "Fans" tool in ANSYS Icepak, which allows the user to set the fan type ("intake"), geometry ("circular"), and flow rate.

Table 1. Heat sink parameters

Parameter	Value
Material	Aluminum (extruded)
Footprint	90 mm × 60 mm
Base thickness	2 mm
Overall height	30 mm
Number of fins	10
Fin thickness	1.5 mm

Figure 1(b) shows a cut-away view of the vapor chamber geometry used for the demonstration. The top surface of the vapor chamber (Surface A) is connected to the heat sink. The bottom surface of the vapor chamber (Surface B) has a centrally located 10 mm × 10 mm heater (labelled H1) with input power of 15 W; the rest of this bottom surface is insulated.

The vapor chamber is implemented in the model as a connected stack of five rectangular blocks: one for the vapor core and two each for the walls and wick layers, as shown in *Figure 1(c)*. The footprint of each block matches the heat sink, and the thicknesses are based on the region the blocks represent (wall blocks 1 and 5 are 100 µm in thickness, wick blocks 2 and 4 are 50 µm, and the vapor core block 3 is 200 µm). Copper thermal properties are selected for the wall material, while custom solid-material properties are defined for the wick and the vapor core. The thermal conductivity of the wick material is set as 40 W/m-K for this demonstration.

For the vapor core, the effective thermal properties are calculated from *Equations (1-2)*. It is important to determine the vapor properties used to evaluate these temperature-dependent effective thermal properties at the average vapor core saturation temperature. This temperature can be guessed or approximated in advance based on the heat sink thermal resistance and then iteratively updated using the predictions. For this example, the properties of water are evaluated at 32°C, resulting in $k_x = k_y =$ 11,019 W/m-K and $k_z = 2.7$ W/m-K for the vapor core (using an accommodation coefficient value of $\sigma = 0.03$ for water). These vapor core effective properties can be defined in ANSYS Icepak

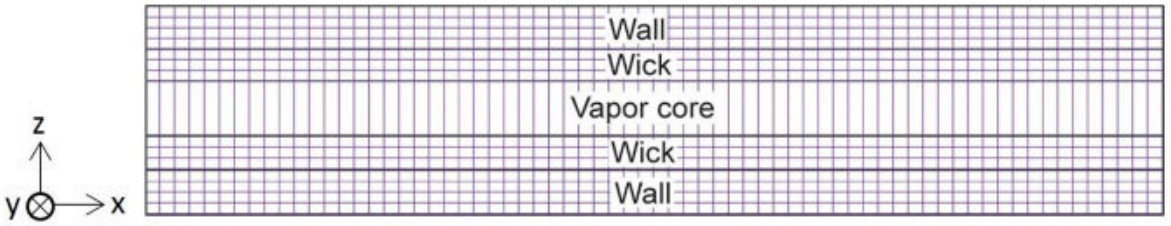

Figure 2. Illustration of the meshing of the vapor chamber.

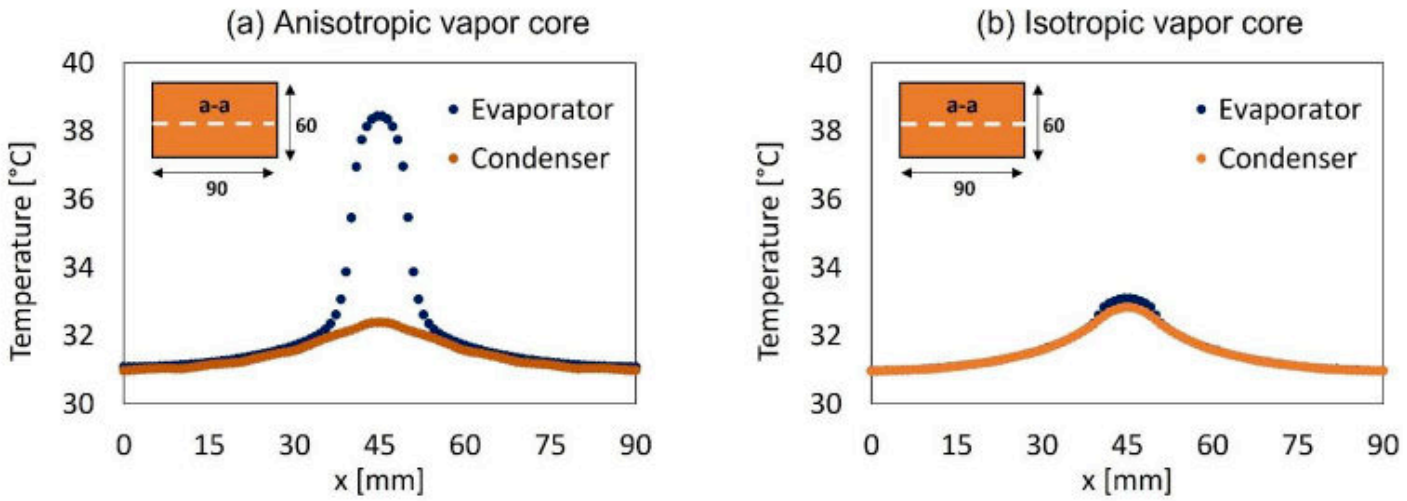

Figure 3. Spatial temperature profile along the line a-a (shown in the inset) along the evaporator and condenser surfaces of the vapor chamber, considering the vapor core as (a) anisotropic ($k_x = k_y$ = 11019 W/m-K, k_z = 2.7 W/m-K) versus (b) isotropic ($k_x = k_y = k_z$ = 11,019 W/m-K).

by selecting a solid material type with a custom orthotropic conductivity, setting the in-plane property (k_x, k_y) to 11,019 W/m-K and the out-of-plane property (k_z) to 2.7 W/m-K, using the coordinate system shown in *Figure 1(b)*.

While meshing the vapor chamber, we reiterate that it is critical to ensure that the mesh of the vapor core has just a single cell across the *z*-direction, as shown in the snapshot of the mesh shown in *Figure 2*. As explained earlier in Section 3, this requirement arises from implementing the effective thermal conductance as a material thermal conductivity in a conduction solver. In ANSYS Icepak, single-cell meshing of the vapor core thickness can be achieved by editing the meshing parameters per-object, and setting the vapor core block to request a z-direction mesh count of 1. Most commercial conduction software has similar provisions for custom-defined mesh constraints. The mesh resolution in the in-plane directions and across the thickness of the other blocks in the domain should follow standard simulation best practices, including confirmation of mesh independence. For purposes of this demonstration, the wall and wick have three and four cell counts across their thicknesses, respectively, as shown in *Figure 2*. The cell counts of all layers in the vapor core are summarized in *Table 2*.

Table 2. Meshing details of the vapor core.

Direction	Cell count
x	200
y	200
z	1

Demonstration Results

Figure 3(a) shows the steady-state temperature profile across the vapor chamber evaporator and condenser surfaces (along the line a-a indicated in the inset) computed by representing the vapor core as an anisotropic conduction block ($k_x = k_y$ = 11,019 W/m-K, k_z = 2.7 W/m-K) as recommended. For comparison, the same temperature profiles are plotted in *Figure 3(b)* when assuming the vapor core to be isotropic ($k_x = k_y = k_z$ = 11,019 W/m-K). When assuming an isotropic vapor core, the maximum temperature on the evaporator at the location of heat input is grossly under-predicted. Considering an ambient air temperature of 20°C, this under-prediction of the maximum evaporator temperature by 6°C corresponds to a 33% error in total thermal resistance of the assembly. *Figure 4* compares the spatial temperature distribution across the evaporator surface

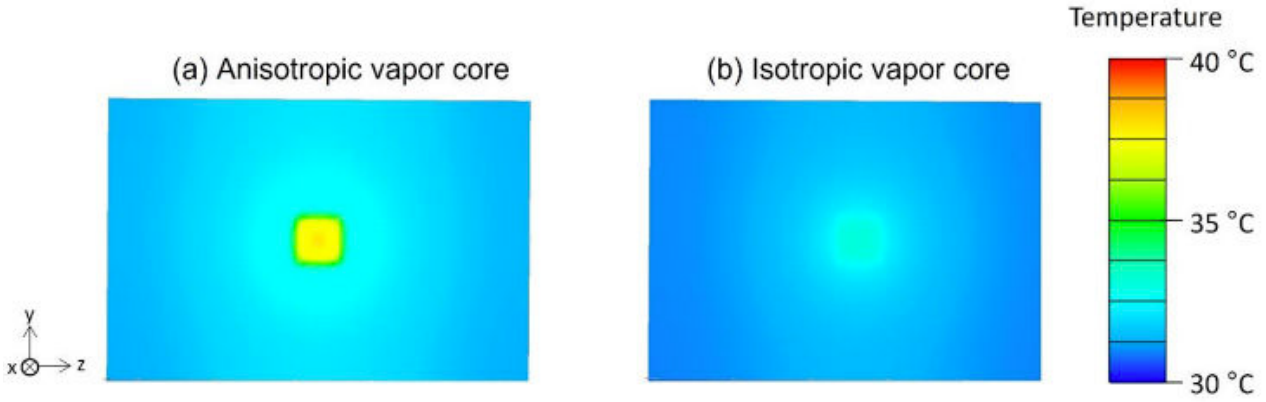

Figure 4. Spatial temperature profile for evaporator (Surface B in Figure 1(b)) of the vapor chamber. Two cases are shown here, with the vapor core considered (a) anisotropic, and (b) isotropic. Modeling the vapor core as isotropic leads to an almost uniform temperature prediction over the evaporator (Surface B), which is clearly incorrect.

for a vapor core represented using anisotropic (*Figure 4(a)*) versus isotropic (*Figure 4(b)*) conduction blocks. It is observed that the evaporator surface temperature for the unphysical representation as an isotropic vapor core is unrealistically uniform compared to the anisotropic vapor core. This demonstration highlights the importance of representing the vapor core with effective anisotropic thermal properties to correctly simulate the physics of vapor chamber transport and predict temperature distributions.

Conclusions

This article provides easy-to-calculate effective properties that allow for prediction of the thermal response of a vapor chamber by representing the vapor core as an anisotropic conduction block. Thermal system designers can thereby simulate vapor chambers, either as standalone devices or within a system, without resorting to complex and computationally expensive direct simulation of the vapor transport. A guide to implementation of these effective properties into numerical conduction solvers is provided, and users of the technique should pay special attention to the following:

- The effective anisotropic properties presented here are derived from an analogy between a simplified physical vapor chamber transport model and the transient heat diffusion equation. Their accuracy is subject to the same assumptions made in the original vapor chamber transport modeling, with further discussion and error bounds provided in Ref. [5].
- The single-cell-thick meshing guidelines for the vapor core should be strictly followed so that values calculated from the expression for kz in *Equation (2)* can be substituted as a cross-plane thermal conductivity in a numerical conduction solver.
- The intrinsic effective properties derived depend only on the working fluid properties and vapor core thickness, and are independent of the boundary condition. However, they are highly sensitive to the vapor core temperature and geometry of the vapor chamber and therefore must be recomputed for new cases and operating conditions.

References

[1] U. Vadakkan, S.V. Garimella, and J. Murthy, "Transport in Flat Heat Pipes at High Heat Fluxes From Multiple Discrete Sources," ASME Journal of Heat Transfer, vol. 126, pp. 347–354.
[2] R. Ranjan, J.Y. Murthy, S.V. Garimella, D.H. Altman, and M.T. North, "Modeling and Design Optimization of Ultrathin Vapor Chambers for High Heat Flux Applications," IEEE Transactions on Components, Packaging and Manufacturing Technology, vol. 2, 2012, pp. 1465–1479.
[3] G. Patankar, J.A. Weibel, and S.V. Garimella, "A Validated Time-stepping Analytical Model for 3D Transient Vapor Chamber Transport," International Journal of Heat and Mass Transfer, vol. 119, 2018, pp. 867–879.
[4] R.S. Prasher, "A Simplified Conduction Based Modeling Scheme for Design Sensitivity Study of Thermal Solution Utilizing Heat Pipe and Vapor Chamber Technology," Journal of Electronic Packaging, vol. 125, 2003, p. 378.
[5] K. Baraya, J.A. Weibel, and S.V. Garimella, "An Effective Anisotropic Properties-Based Representation of Vapor Chambers," IEEE Transactions on Components and Packaging Technologies, vol. 11, 2020, pp. 51–56.
[6] D.S. Smith, A. Alzina, J. Bourret, B. Nait-Ali, F. Pennec, N. Tessier-Doyen, K. Otsu, H. Matsubara, P. Elser, and U.T. Gonzenbach, "Thermal Conductivity of Porous Materials," Journal of Materials Research, vol. 28, 2013, pp. 2260–2272.

Hydraulic and Thermal Characteristic of a Double-Sided Cold Plate. Part 1: CFD Analysis

Azita Soleymani
Meta

William Maltz
President of Electronics Cooling Solutions Inc.

John Wilson
Siemens Digital Industries Software

Introduction

Many programs geared toward the design of autonomous vehicles have been initiated in recent years. Waymo, Cruise, Baidu, Argo AI, Uber, Lyft, and Tesla are among the innovative self-driving car companies. Advances in autonomous technologies will require enhanced thermal protection of critical electronics to ensure optimized performance, health, and lifetime.

Emerging intelligent autonomous systems are increasingly complex while also required to have smaller size and weight. Packing more functionality into smaller footprints increases the heat density and thermal challenges. As shown in *Figure 1*, liquid cooling has been effectively leveraged to meet Artificial Intelligence (AI) digital electronics requirements in Tesla vehicles.

In this study, the hydraulic and thermal characteristics of the Tesla Autopilot HH2.5 Model 3Y module were investigated in detail. Two units were used in the study. The unit housing and the attached boards were removed to access the cold plates. One of the two cold plates was cut in half so that detailed internal dimensions, locations of the fins, inlet/exhaust ports, pedestals, and cold-plate channels could be measured. The information was used to generate a reliable CAD representation of the cold

Dr. Azita Soleymanin
Dr. Azita Soleymani is a member of the technical staff at Meta, where she applies her skills to manage the thermal aspects of Augmented Reality (AR) products. Dr. Soleymani has a track record of co-authoring over 40 technical papers, reflecting her broad expertise in thermal design. Her proficiency extends to power electronics, consumer electronics, lithium-ion batteries, medical devices, and automotive equipment. Prior to joining Meta, Dr. Soleymani served as a director at Electronic Cooling Solutions Inc. Her responsibilities included providing thermal management guidance to diverse industries.

William Maltz
William Maltz is the president and founder of Electronic Cooling Solutions Inc. (ECS) and has nearly 40 years of experience working on and solving thermal management problems for electronics companies. Prior to working as a consultant, Mr. Maltz worked as a thermal engineer for Tandem Computers and the Amdahl Corporation. He serves on the steering and program committees for the SEMI-THERM symposium the Thermal Technology Workshop and is the section Vice-President of the Santa Clara Valley section of the American Society of Mechanical Engineers. Mr. Maltz received his Bachelor of Science Degree in Mechanical Engineering from San Jose State University.

John Wilson
John Wilson is Electronics Thermal Applications Specialist at Siemens Digital Industries Software. His specialties include electronics thermal design, thermal comfort design, and thermal characterization of ASICs and other IC packages. He has served as Technical or Project Lead in thermal/airflow design and characterization services for over 30 clients and over 100 projects ranging from IC packages through clean rooms. John currently works with product management teams to provide electronics thermal design solutions to leading electronics industry clients globally.

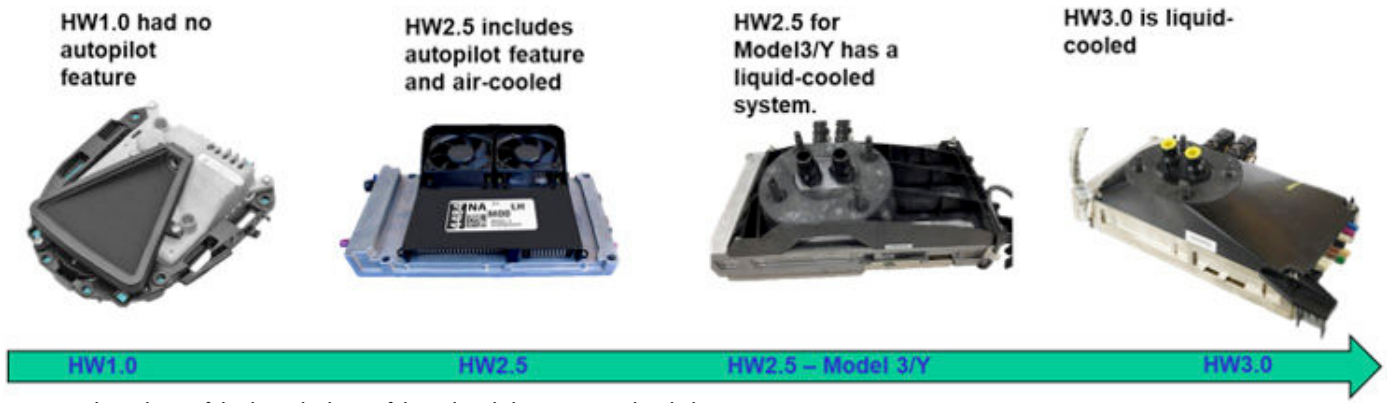

Figure 1. The evolution of the thermal solution of the AI digital electronics in Tesla vehicles

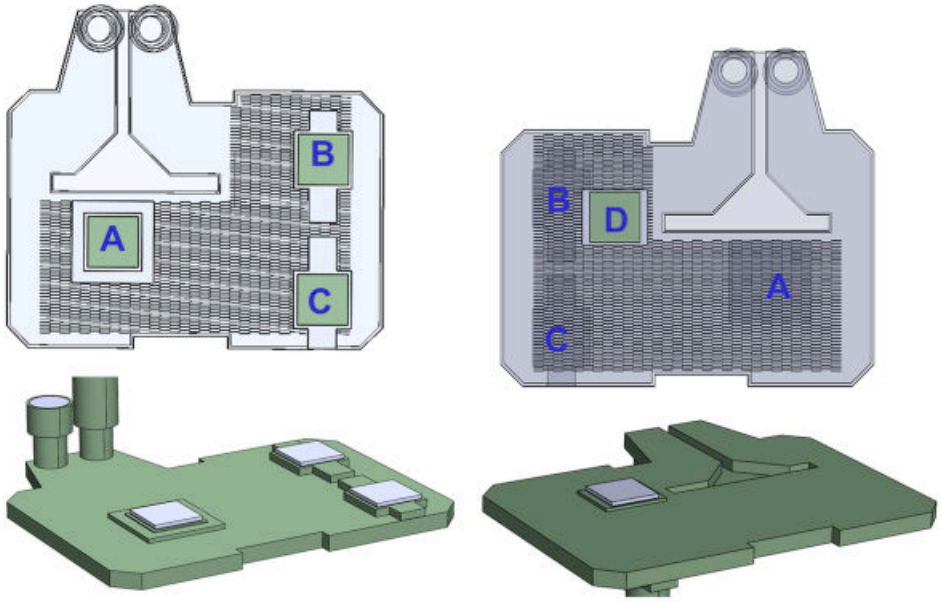

Figure 2. The illustration of the computational domain

plate. A test vehicle was constructed using the second cold plate so that hydraulic pressure drops and thermal performance could be measured.

A computational fluid dynamics (CFD) model was constructed using commercial software [1] to evaluate the cold plate used in the test module. The CFD model was run with equivalent heat loads placed at the same locations as in the test vehicle and with fluid flowing at the same rate as in the experimental setup unit. The CFD results were then compared to the test data. A good correlation between the test data and the simulation results was found.

Part 1 of this set of articles describes the construction of the CFD model and the simulation results that examined the hydraulic and thermal performance of the cold plate across a range of operating conditions. Part 2 will include the step-by-step tear-down process of the unit, the experimental set-up, validation of the CFD model, and a description of the development and use of thean Artificial Neural Network of the cold plate assembly to study the performance of the system at a wide range and combinations of the operating parameters.

Numerical Simulations

CFD simulations were carried out using the commercial code and assuming that the flow and temperature fields were steady state. The continuity and momentum equations along with the energy equation were solved numerically for the pressure, velocity, and temperature fields using the finite volume method. To divide the computational domain into discrete control volumes, more than 1.5 million non-uniform 3D tetrahedral computational cells were used.

As shown in *Figure 2*, four 25.4 x 25.4 mm die were mounted to the cold plate. These die locations are labeled to provide reference points for the discussion in this article.

To study the thermal performance of the cold-plate, a constant heat load of 125.5 W was applied to each of the 25.4 mm x 25.4

mm x 2 mm rectangular prisms representing the chips located on the cold plate pedestal. A Network Resistance model was assigned to each heater representing the chips. The junction-to-case and the junction-to-board resistances were set at 0.1 and 1,000 $^oC/W$, respectively to ensure that the heat dissipated by each chip was rejected to the cold plate. A thermal interface material with a thickness of 0.25 mm and a thermal conductivity of 10 W/m-K was placed between the cold plate and the heaters. The liquid was assumed to be 50/50 Glycol/water with constant heat capacity, density, thermal conductivity, and viscosity of 3,800 J/kg-K, 1040 kg/m^3, 0.36 W/m-K, and 0.006 N-s/m^2, respectively.

Results and Discussion

Contour plots of the temperature and velocity fields are illustrated in *Figures 3* and *4* to provide insight into the performance of the cold plate and to identify opportunities for design improvements. Coolant inflow temperature and the flow rate were set to 30^{o}C and 5.2 liters per minute (LPM), respectively. The cold plate thermal conductivity was 113 W/m-K and the thermal load per chip was set to 125.5 W. The region with no fins had the lowest hydraulic impedance. Therefore, as shown in *Figure 3*, a large percentage of the coolant bypassed the chips and exited the cold plate without making a significant contribution to the heat removal. The flow through the bypass increased with length, indicating that the flow was leaking from the fin stack along the length to the bypass region. The average velocities in the vicinity of Chips B (0.4m/sec) and D (0.3m/sec) were higher than in the vicinity of Chips A (0.2 m/sec) and C (0.2m/sec).

The average bulk temperature of the coolant at the exhaust side of the cold plate was 31.4^{o}C. The average temperature of the coolant beneath Chips B and D was higher than the average liquid bulk temperature. This is illustrated by the fluid particle trajectories shown in *Figure 5*.

Cold fluid by-passed Chip A and approached Chip C. Therefore, the average temperature of the fluid as it approached Chip C was independent of the power dissipation of Chip A and could be approximated by the coolant inlet temperature. Chips B and D are located downstream of fluid that passed beneath Chips A and C. The heat dissipated by Chips A and C was exhausted from the cold plate into the fluid before the fluid approached the region in the cold plate below Chips B and D. High power dissipation by Chips A and C and/or a lower fluid flow rate results in a higher fluid temperature as the fluid approaches Chips B and D. This in turn results in higher temperature for Chips B and D as compared with the temperature of Chips A and C.

Some of the liquid trajectories beneath Chips B and D take a V-shape path as they pass through the cold plate. The result is a longer contact time with the die and therefore a higher temperature for those particle trajectories.

The temperature contour plots of the chips and the cold plate are shown in *Figure 6*. The maximum temperature difference be-

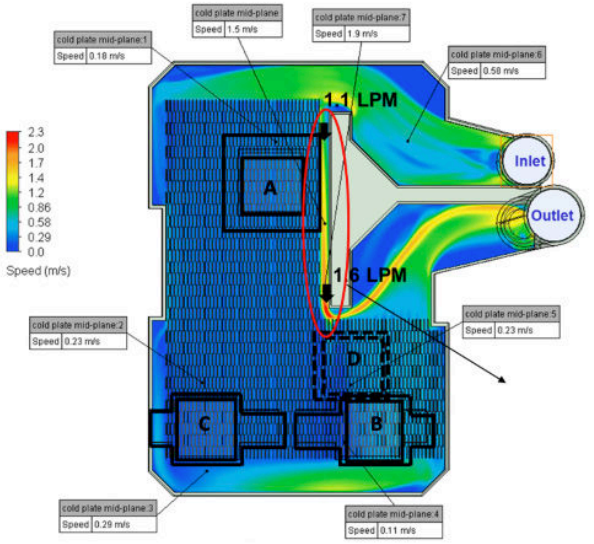

Figure 3. Velocity Contour Plot at the Midplane of the Cold Plate; Over 1.1 LPM out of 5.2 LPM of coolant by-passes the electronics and exits the cold plate without contributing to the cooling

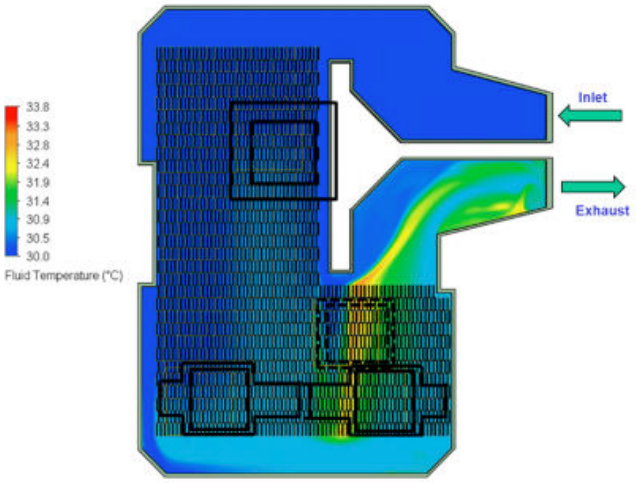

Figure 4. Temperature Contour Plot at the Midplane of the Cold Plate

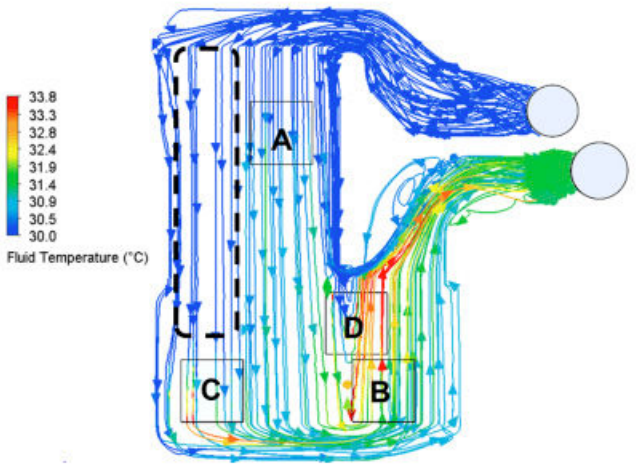

Figure 5. Velocity Vector Colored by Magnitude of Coolant Temperature

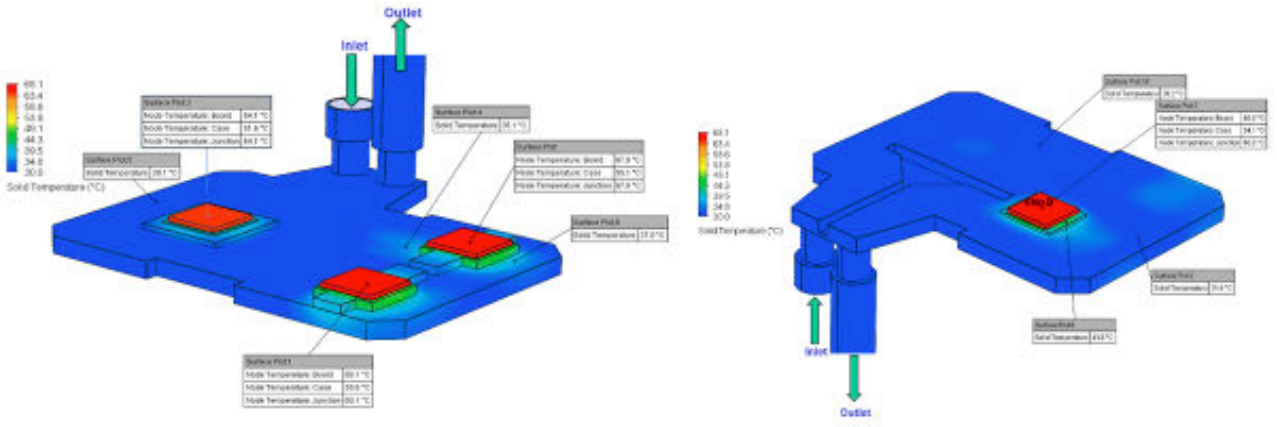

Figure 6. Temperature Profile of the Chips (a) front-side and (b) back-side views

	Pedestal surface Area (mm^2)	Pedestal thickness, (mm)	Average velocity beneath the chip, (m/s)	Average fluid temperature beneath the chip (°C)	Die junction temperature (°C)
Chip A	1681	2.3	0.2	30	64.1
Chip B	1219	3.9	0.4	32.2	67.6
Chip C	1219	3.9	0.2	30	68.1
Chip D	924	1.6	0.3	31	66.6

Table 1.

tween the four chips was 4°C. The cold plate can remove 4 x 125.5 W = 502 W from these chips while maintaining chip junction temperatures well below the temperature limit of 90°C.

For a given flow rate, assuming identical power load, dimensions, and TIM for all four chips, the temperatures of the chips depend on four interrelated factors: the thickness and surface area of the pedestal, cold plate flow distribution, and fluid temperature in the vicinity of the chip. The effect of the pedestal presumably is a combination of thickness and area since it acts as both a vertical conductor and horizontal spreader. Theoretically it is expected that the temperature of the chip increases with an increase in the thickness of the pedestal or the coolant temperature beneath the chip. Furthermore, the temperature of the chip is expected to increase with a decrease in the surface area of the pedestal or the velocity of the coolant beneath the chip. *Table 1* summarizes the impact of the four interrelated factors on the chip temperatures.

From conservation of energy, the greater the coolant flow rate, the smaller the gradient of the coolant temperature across the cold plate. The temperature increase of the coolant across the cold plate as a function of the coolant flow rate is shown in *Figure 7*.

As shown in *Figure 8*, chip temperatures increase with a decrease in the coolant flow rate. The study shows that chip temperatures were dependent on the flow rate. Chip temperatures began to increase dramatically once the flow rate went below 4 LPM. The temperature variations between the chips also increased as the coolant flow rate decreased. The difference in chip temperature was 4°C and 12°C at 10 LPM and 1 LPM, respectively. Chips from the lowest to the highest temperatures were A, D, B, and C, for flow rates above 4 LPM.

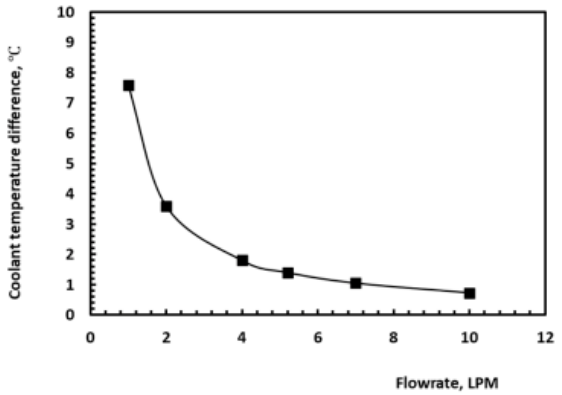

Figure 7. The temperature increase of the coolant across the cold plate

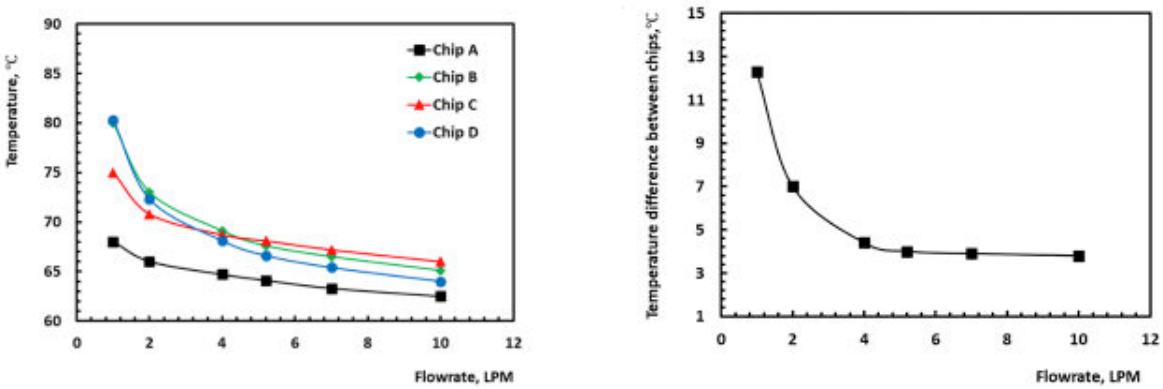

Figure 8. (a) Temperature of the chips at different flow rate (b) maximum temperature difference between the chips as a function of coolant flow rate

Conclusion and Summary

In this study, the hydraulic and thermal characteristics of an autopilot module were investigated in detail. The unit includes a double-sided cold plate with circuit boards attached to each side of a cold plate. One unit was torn down to measure the detailed internal dimensions, locations of the fins, inlet/exhaust ports, pedestals, and cold-plate channels. That information was used to generate a 3-D numerical model of the module using commercial CFD software. Results from simulations that examined the hydraulic and thermal performance of the cold plate are presented in this article. The follow-on article, Part 2, will include a step-by-step description of the tear-down process of the unit and the experiments that measured the hydraulic head loss through the cold plate and evaluated the thermal performance at several coolant flow rates and power loads. The test results were used to validate the CFD model. It will be shown that the model results for the hydraulic pressure loss and temperature profiles were consistent with the experimental data. An Artificial Neural Network (ANN) of the cold plate assembly was then developed using the CFD results presented in this paper. The ANN model was used to study the performance of the system at a wide range and combinations of the operating parameters. In Part 2, it will be demonstrated that the developed ANN model could be used to determine the performance limit of the cold plate.

References

[1] Simcenter Flotherm XT 2021.1, Siemens Inc., https://plm.sw.siemens.com/en-US/simcenter/fluids-thermal-simulation/flotherm-xt/

Rank Sum Tests

Ross Wilcoxon
Associate Technical Editor for *Electronics Cooling*
Collins Aerospace

Introduction

The previous column in this series described methods for assessing whether a set of data was normally distributed [1]. In the event that data is shown to not have a normal distribution, one might ask how to conduct a statistical analysis on it given that many statistical tests are developed on the assumption that the data are normal. For example, how can two non-normal data sets be analyzed to determine whether one is statistically better than the other?

Nonparametric statistics is used to analyze data that are not well described by discrete parameters, such as the mean and standard deviation used to describe a normal distribution. One useful method in nonparametric statistics is the Wilcoxon Rank Sum (WRS) Test[1], which is also known as the Mann-Whitney-Wilcoxon test. The WRS test analyzes the ranks of an ordered data set rather than the direct values of actual values. This is analogous to how the median may provide a more representative assessment of a population than the mean, if the data set includes a few extreme values (such as in determining the typical net worth of a small group of people that happens to include a billionaire).

Rank Sum Test Procedure

The WRS test procedure begins by combining two data sets and sorting them in order of lowest to highest values (sorting from highest to lowest also works). The ranks of each value in the sorted values for each data set are then added together. In the event that two or more values have the same rank, then they are all assigned the same average rank.

Consider the two data sets (A and B) shown in *Table 1*, which includes a total of ten measurements (4 in Data Set A and 6 in Data Set B). The largest term in the combined list of data is the value of 5.1 in Data Set B, so it has a rank of 1 (as shown in the column on the right edge of the figure). Data Set A includes the smallest measurement of 3.2, which corresponds to the 10th rank in the combined data set. Data Set B includes two values of 4.1, which ranks 3rd in the combined list. Since these two would occupy ranks 3 and 4 in the list, they are each assigned the average rank of 3.5.

	Data		Ranks	
	A	B	A	B
	4.0	5.1	5	1
	3.6	4.3	7.5	2
	3.5	4.1	9	3.5
	3.2	4.1	10	3.5
		3.8		6
		3.6		7.5
total	14.3	25	31.5	23.5
count	4	6		
average	3.58	4.17		
st dev	0.33	0.52		

Table 1. Example Data Set

Once the rank for each data value has been assigned, the ranks are added together. For example, the ranks for Data Set A are 7.5+5+10+9=31.5 and the rank sum for Data Set B is 23.5. The rank sum value for the data set with the smallest number of terms is then compared to the WRS critical values for a given probability value.

Table 2 shows a set of WRS critical values for a 5% one-sided distribution (and 10% two-sided distribution for values of m and n, where m is the number of values in the data set with the fewest terms and n is the number of terms in the other data set.

n =	m=3	m=4	m=5	m=6	m=7
m	6, 15	12, 24	19, 36	28, 50	39, 66
m+1	7, 17	13, 27	20, 40	30, 54	41, 71
m+2	7, 20	14, 30	22, 43	32, 58	43, 76
m+3	8, 22	15, 33	24, 46	33, 63	46, 80
m+4	9, 24	16, 36	25, 50	35, 67	48, 85
m+5	9, 27	17, 39	26, 54	37, 71	50, 90
m+6	10, 29	18, 42	27, 58	39, 75	52, 95
m+7	11, 31	19, 45	29, 61	41, 79	54, 100

Table 2. Wilcoxon Rank Sum Critical Values for probability of 5% (one sided), from [3]

[1] The individual who first developed the WRS test [2] was not related to the author

For the case corresponding to the data in *Table 1*, the critical values for m=4 and n=m+2=6 are found in Table 2 to be 14 and 30. The rank sum for Data Set A was calculated as 31.5, which is outside the range of 14-30. Therefore, one can conclude to a 90% confidence level that Data Set A is different from Data Set B, i.e., that the higher values of Data Set B relative to Data Set A is statistically significant.

Note that if the data were analyzed using a conventional t-test, the same conclusion with a similar confidence level would be found. However, if the maximum value of 5.1 in Data Set B were replaced with a much larger value of, for example, 10, the t-test would conclude that the two data sets were not statistically different due to the substantially larger variance in Set B. Because the impact of a single value in a data set is lessened in larger data sets, differences in the results for a t-test and a WRS test are generally insignificant when sample sizes for a single data set are larger than 15-20.

How WRS Critical Values are Found

Since nonparametric tests like the WRS test are not dependent on assumptions regarding the distribution and are less influenced by individual outlier data points, one might ask why the WRS test is not always used instead of a test such as the t-test. One likely reason is that there is no simple method for determining the WRS test critical values. Typically, those values are found from a table such as that shown in *Table 2* or more extensive tables such as Reference [4]. Readers who are content with simply using terms listed in a critical value table, may choose to skip the rest of this section. Those readers who, like this author, are bothered by 'magically appearing' terms and want to better understand how the critical values are generated, may choose to read on.

The WRS critical values are generated by determining the rank sums that could result from every combination of a data set with a given size. For example, consider two data sets for A and B where each set only includes 2 values. The number of possible combinations of ranks that could be generated is found with the 'n choose k' formula that determines how many combinations of k terms can be generated with n variables. With this equation, the number of possible combinations of ranks is (n+m)!/(n!*m!), so for the case of n=m=2, the number of combinations is (1*2*3*4)/(1*2)/(1*2) = 6. These six possible combinations are shown in *Table 3*; for Combination 1, for example, the two highest largest terms are from set A and the smallest two terms are from set B. This table also shows the rank sums for each combination for the two data sets.

Table 4 shows the probability and cumulative distributions of each rank sum, which are the number of occurrences equal to and less than or equal to that rank sum, respectively, divided by the number of combinations.

Figure 1 plots the values shown in the last column on *Table 4* for m=n=2 (with symbols and a line) as well as lines that show the

		Rank					Rank Sum	
		1	2	3	4		A	B
Combinations	1	A	A	B	B		3	7
	2	A	B	A	B		4	6
	3	A	B	B	A		5	5
	4	B	A	A	B		5	5
	5	B	A	B	A		6	4
	6	B	B	A	A		7	3

Table 3. Combinations for n=m=2

Rank Sum	# of times	distribution	
		probability	cumulative
2	0	0%	0%
3	1	16.7%	16.7%
4	1	16.7%	33.3%
5	2	33.3%	66.7%
6	1	16.7%	83.3%
7	1	16.7%	100%

Table 4. Probability and Cumulative Distributions for m=n=2 Combinations

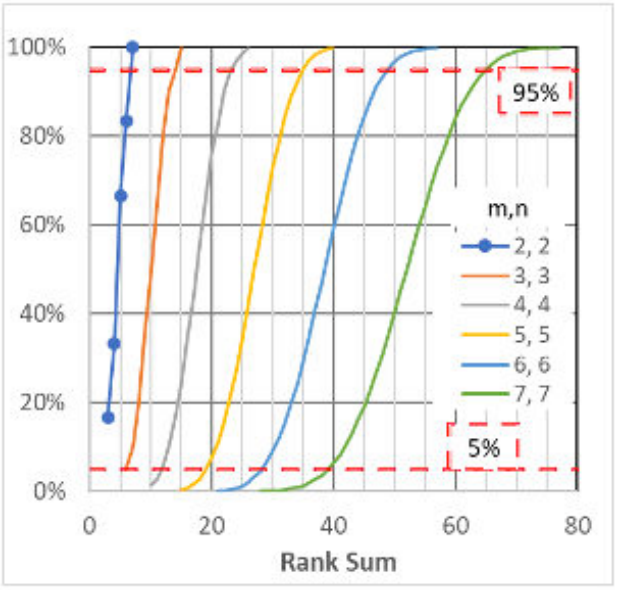

Figure 1. Distributions for m=n= 2 and 3

[2] The table shows values at a 5% confidence level for a single-sided distribution, so the overall confidence level is reduced because the distribution is two-sided.

cumulative distributions for m=n=3, 4, 5, 6, and 7. The figure also includes horizontal lines for cumulative probabilities of 5% and 95%. The intersections of these horizontal lines with the cumulative distributions correspond to the WRS critical values. For example, the m=n=7 distribution intercepts the 5% and 95% lines at Rank Sum values of approximately 40 and 65, respectively. Those values agree well with the terms shown in Table 2 of 39 and 66 (in the upper right-hand cell of the table).

While the process of calculating the WRS critical values is straightforward, it can be computationally intensive. To calculate the critical values for m=n=7, for example, includes accounting for 14!/(7!*7!) = 3432 combinations. Doubling the number of terms to m=n=14 increases the number of combinations to evaluate to more than 40 million.

As the number of data points increase, the WRS distributions more closely approximate a normal distribution. The differences between the distributions become increasingly isolated to the extreme tails.

Summary

Data may not always be easily characterized with a parametric distribution such as the normal distribution. In those cases, non-parametric tests like the Wilcoxon Rank Sum test may be used. This test can serve a similar role as the t-test, but uses the ranks of terms in the combined data set, similar to a median value, rather than average and standard deviations of data sets.

Because the method for calculating the WRS critical values can require substantial computational power, it is typical that these values are found in a table. As the size of the samples increases, the WRS distributions used to calculate the critical values more closely approximate a normal distribution. Therefore, when the total number of samples gets larger than ~20-30, the impact of using the WRS test or assuming a normal distribution will likely become negligible. In those cases, it may become important to identify outliers that have an excessive influence the results. This is the topic of the next article in this series.

References

[1] Previous statistics corner
[2] https://en.wikipedia.org/wiki/Frank_Wilcoxon
[3] Milton & Arnold, "Probability and Statistics in the Engineering and Computing Sciences, McGraw-Hill, Inc., 1986
[4] https://users.stat.ufl.edu/~winner/tables/wilcoxonmannwhitney%5B1%5D.pdf


Call for Authors
and Contributors!
Want to be a part of the next issue of Electronics Cooling? Have an article or blog post you'd like to write for Electronics-Cooling.com?
Let us know at
editor@electronics-cooling.com
electronics COOLING
www.Electronics-Cooling.com

Index of ADVERTISERS

SIEMENS Digital Industries Software
8005 SW Boeckman Road
Wilsonville, OR 97070

t: (800) 592-2210
e: www.plm.automation.siemens.com/global/en/contact-us.html
w: www.plm.automation.siemens.com/global/en/
page: 2

Electronics Cooling
1000 Germantown Pike,
Plymouth Meeting, PA 19462

t: 484.688.0300
e: info@electronics-cooling.com
w: electronics-cooling.com
page: 30

LECTRIX
1000 Germantown Pike
Plymouth Meeting, PA 19462

t: (484) 688-0300
e: info@lectrixgroup.com
w: lectrixgroup.com
page: 32

ThermalLIVE Summit
Online Event
May 9, 2023

t: (484) 688-0300
e: info@electronics-cooling.com
w: thermal.live
page: 11


Break the same old pattern.
Problem First. Product Last.
Content | Data | Marketing Technology
LECTRIX®
Digital Marketing for the B2B Electronics Industry
1.484.688.0300 | info@lectrixgroup.com
www.lectrixgroup.com